ISSN: 2161-6795 Volume 8, Number 4, October 2018

Scientific Research Publishing

World Journal of Nuclear Science and Technology

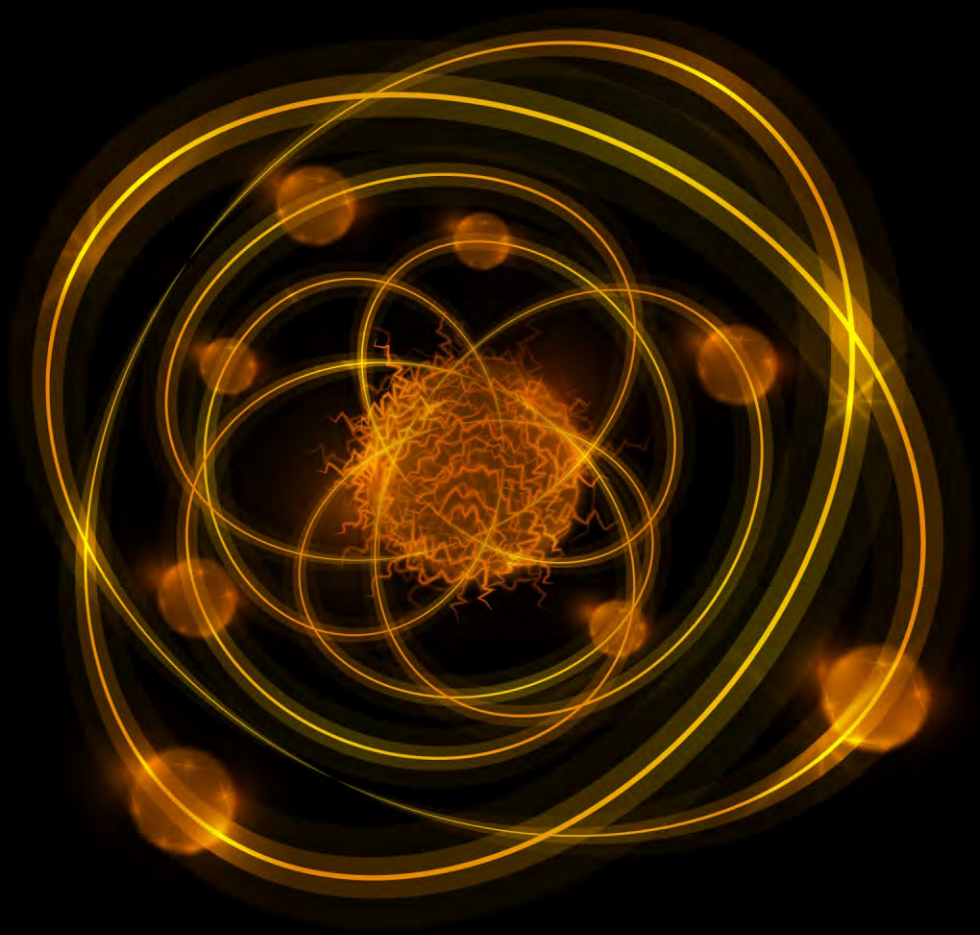

ISSN: 2161-6795

www.scirp.org/journal/wjnst

Journal Editorial Board

ISSN 2161-6795 (Print) ISSN 2161-6809 (Online)
http://www.scirp.org/journal/wjnst

Editor-in-Chief

Editorial Board

World Journal of Nuclear Science and Technology, 2018, 8, 147-196
http://www.scirp.org/journal/wjnst
ISSN Online: 2161-6809
ISSN Print: 2161-6795

Table of Contents

Volume 8 Number 4 October 2018

World Journal of Nuclear Science and Technology (WJNST)
Journal Information

SUBSCRIPTIONS

The *World Journal of Nuclear Science and Technology* (Online at Scientific Research Publishing, www.SciRP.org) is published quarterly by Scientific Research Publishing, Inc., USA.

Subscription rates:
Print: $79 per issue.
To subscribe, please contact Journals Subscriptions Department, E-mail: sub@scirp.org

SERVICES

Advertisements
Advertisement Sales Department, E-mail: service@scirp.org

Reprints (minimum quantity 100 copies)
Reprints Co-ordinator, Scientific Research Publishing, Inc., USA.
E-mail: sub@scirp.org

COPYRIGHT

PRODUCTION INFORMATION

For manuscripts that have been accepted for publication, please contact:
E-mail: wjnst@scirp.org

World Journal of Nuclear Science and Technology, 2018, 8, 147-159
http://www.scirp.org/journal/wjnst
ISSN Online: 2161-6809
ISSN Print: 2161-6795

Reexamination of the Claim of Marinov *et al.* on Discovery of Element 112

S. R. Hashemi-Nezhad[1], Reinhard Brandt[2], Wolfram Westmeier[2,3]

[1]School of Physics, University of Sydney, NSW 2006, Australia
[2]Kernchemie, FB Chemie, Philipps Universität, Marburg, Germany
[3]Dr. Westmeier GmbH, Ebsdorfergrund, Germany
Email: reza.hash@sydney.edu.au

How to cite this paper: Hashemi-Nezhad, S.R., Brandt, R. and Westmeier, W. (2018) Reexamination of the Claim of Marinov *et al.* on Discovery of Element 112. *World Journal of Nuclear Science and Technology*, **8**, 147-159.
https://doi.org/10.4236/wjnst.2018.84013

Received: August 16, 2018
Accepted: September 24, 2018
Published: September 27, 2018

Abstract

Marinov *et al.* have detected spontaneous fission events in sources separated from tungsten targets irradiated with 24 GeV protons. These fission events could not be attributed to actinides or to any other known isotope. Marinov *et al.* propose that fission events are due to production of element 112 (Eka-Hg) in the tungsten target. We have addressed Marinov's claim with a new analysis of their data and modern theoretical model calculations of possible interactions. Using data available in the literature the spontaneous fission half-life of the Eka-Hg was estimated to be ~74 days. This is dramatically longer than the half-life obtained for $^{283}_{112}\mathrm{Cn}$, produced in the fusion of energetic $^{48}\mathrm{Ca}$ ions with $^{238}\mathrm{U}$. Monte Carlo calculations show that enough Sr isotopes are produced in the tungsten target to make the production of element 112 via fusion of Sr and W feasible; however, if such fusion was possible it had to be deep sub-barrier fusion.

Keywords

Element 112, Tungsten Target, Spallation Products, Heavy Ion Fusion

1. Introduction

Forty seven years ago Marinov *et al.* [1] [2] [3] reported evidence for possible synthesis of a super heavy (SH) element (Z = 112) in the irradiation of tungsten target with 24 GeV protons.

They irradiated three W-targets, each with mass of 33 g and thickness 120 g·cm^{-2} using the CERN PS accelerator. These targets are referred to as W1, W2 and W3. Table 1 gives some information on irradiation of the targets [1]. The W1 target was available for analysis 3 - 4 month after the end of the irradiation.

Table 1. Irradiation data for three tungsten targets from [1].

Target	Irradiation period	Number of protons on target	Time between end of irradiation and start of analysis
W1	About a year	2×10^{18}	3 to 4 months
W2	About 4 months	7×10^{17}	A few days
W3	NA	NA	NA

For reasons given in [1] most of the reported experimental results and findings are for W2-target and we will focus on this target as well.

The synthesis of isotope ${}^{283}_{112}\mathrm{Cn}$ of element 112 via ${}^{48}_{20}\mathrm{Ca} + {}^{238}_{92}\mathrm{U} \rightarrow {}^{286}_{112}\mathrm{Cn} \rightarrow {}^{283}_{112}\mathrm{Cn} + 3\mathrm{n}$ reaction was reported in 1999 [4] [5]. Prior to that in 1996 [6], production of ^{277}Cn in ^{208}Pb (^{70}Zn, n) reaction has been reported. The half-life of ^{283}Cn is 4 s and ^{277}Cn has a half-life of 0.69 ms.

Discovery of the short-lived isotopes of element 112 does not rule out the existence of long-lived isotopes of this element.

Marinov *et al.* [1] [2] [3] suggest that neutron deficient long lived isotopes of element 112 can exist and may be produced with higher cross-sections.

Their claim is based on the following assumptions and observations:

1) Element 112 would be a chemical homologue of mercury (Eka-Hg).

2) Detection of spontaneous fission events in Eka-Hg sources separated from proton irradiated W-targets, which could not be attributed to actinides or to any other known isotope.

Heavy ion fusion experiments such as [4] [6] obviously will not be able to detect the long-lived SH isotopes because very few atoms of these are produced. On the other side, experiments like that of the Marinov *et al.* will not be able to detect the short-lived SH isotopes because of the required long chemical separation times.

Several attempts to reproduce the experimental findings of Marinov *et al.* were inconclusive, see e.g. [7] [8] [9] [10]. The rejection by Barber *et al.* [11] of the claim of Marinov *et al.* was recently addressed by Brandt *et al.* [12] who point out that presently unexplained findings may indicate novel reaction paths leading to unexpected results.

In this paper we use the experimental results given in the publications of Marinov *et al.* to investigate the feasibility of reproducing their findings in possible future experiments.

2. Calculation of Spontaneous Fission Half-Life of Eka-Hg

Table 2 gives a timeline of the experiments and measurements on W2 target after the end of the proton irradiation, taken mainly from [1]. For those periods where no information was available in the literature, reasonable times have been assigned by us. The timeline given in the last column of **Table 2** is used in this report.

The most unambiguous experimental results reported [1] are the fission

Table 2. Timeline of experiments and measurements after the end of the irradiation.

Chemical separation and alpha activity measurements			
Row number	**Description**	**Experimental times from Ref. 1**	**Times used in the calculations**
1	Time from end of irradiation to start of chemical separation	A few days	4 d
2	Chemical separation period	NA	2 d
3	Alpha counting of Eka-Hg source from W2	406 h (16.92 d)	16.92 d
4		236 h (9.83 d)	9.83 d
5	Time interval between two alpha counting (3 and 4 above)	24 d	24 d
6	Alpha counting of Eka-Hg source from W1 sample	280 h (11.7 d)	11.7 d
7	Time gap between alpha counting of the W2 and W1 sources	NA	0.5 d
8	Background alpha counting	10 d	10 d
9	Total time from end of irradiation to end of alpha counting	NA	79 d
	Fission event detection		
10	Time gap between end of alpha counting and start of fission track recording	NA	0 d
11	First Makrofol foil exposure	7 d	7 d
12	Second Makrofol foil exposure	14 d	14 d
13	Time gap between two exposures	4 d	4 d
14	Time spent for thickness reduction of Eka-Hg source from W2	NA	1 d
15	First Makrofol foil exposure (reduced sample thickness)	8 d	8 d
16	Second Makrofol foil exposure (reduced sample thickness)	8 d	8 d
17	Time gap between two Makrofol exposures	13 d	13 d

events recorded after attempts to reduce the thickness of the Eka-Hg source prepared from W2 target, (Table 2, rows 15 - 17). The spontaneous fission half-life of Eka-Hg can be calculated using these data.

The fission events in the source were recorded as tracks in Makrofol KG polycarbonate foils (hereafter referred to as Makrofol) that were placed in close contact with the surface of the source.

First of all one need to convert the observed fission tracks in the Makrofol foils to the number of fission events in the source.

Fission track density ρ (tracks cm^{-2}) in a foil in contact with a fission source is related to the number of fission events per unit volume of the source, N_v by the following relationship [13] [14]

$$\rho = n\varepsilon\mu dN_v \tag{1}$$

where:

n is number of fragments per fission event (we use $n = 2$);

ε is fission track detection efficiency of Makrofol foil which is ~1;

μ is a parameter that depends on fission source thickness d and range of the fission fragments in the source material, R.

For a thin source ($d < R$) equation 1 can be written as

$$N_c = \eta N_f \tag{2}$$

where N_c is total number of fission tracks detected in the Makrofol foil, N_f is number of fission events in the source and η *is*

$$\eta = n\varepsilon\mu \tag{3}$$

For a thin source, μ is given by [13] [14]

$$\mu = \frac{1}{2}\left(1 - \frac{d}{2R}\right) \tag{4}$$

Determination of μ requires knowledge of source thickness, and range of fission fragments. The authors of [1] mention that the thickness of the Eka-Hg source was 2 mg·cm^{-2}, but the density of the source material is not given. If we assume that source material has a density equivalent to the density of HgO (11.14 g·cm^{-3}), thickness of the source and range of fission fragments in the source material may be calculated as 1.8 μm and 8 μm, respectively.

Using the Equation (4) and values of n and ε we obtain $\eta = 0.89$.

The first Makrofol foil was in contact with W2 source for 8 days and showed 28 tracks (row 15 of **Table 2**). Thus

$$\frac{28}{\eta} = N_1\left(1 - \mathrm{e}^{-8\lambda}\right) \tag{5}$$

where N_1 is the number of Eka-Hg nuclei in the source at the start of the 1st Makrofol exposure (row 15 of **Table 2**) and λ is the spontaneousfission decay constant.

The second Makrofol exposure (row 16 of **Table 2**) started 13 days after the end of the first one and the number of tracks in this foil after 8 days of exposure was 23. The number of Eka-Hg nuclei at the start of the second exposure is

$$N_1' = N_1\mathrm{e}^{-(8+13)\lambda}$$

Thus for the second Makrofol exposure we get

$$\frac{23}{\eta} = N_1\mathrm{e}^{-21\lambda}\left(1 - \mathrm{e}^{-8\lambda}\right) \tag{6}$$

From Equations (5) and (6) we obtain: $\lambda = 9.37 \times 10^{-3}$ d^{-1} and $t_{1/2} \approx 74$ d.

The number N_1 of Eka-Hg at the start of the fission track measurements can be calculated using Equation (5) or Equation (6);

$$N_1 = 436$$

Taking into account that fission track recording (row 15 of **Table 2**) started 105 days after the end of the irradiation, the number of Eka-Hg at the end of the irradiation was:

$$N = 1165$$

This number must be corrected for the number of the produced Eka-Hg nuclei that have decayed in the course of the 4 month irradiation period.

The total number of 24 GeV protons that was delivered to W2 target from the PS accelerator of CERN in late 1960s was 7×10^{17}. With a pulse repetition time of 2.4 s and number of protons per pulse of 10^{12} [15] [16] total actual target exposure time has been ~1.68×10^6 s (~19 days). This implies that ~84% of the irradiation time (~4 month) the target did not receive any proton while the produced Eka-Hg nuclei were decaying. Therefore a large number of the nuclei of interest have been lost prior to the start of chemical separation. An accurate calculation of this lost activity requires knowledge of the exact timeline of the irradiation and pulse intensity distribution during the irradiation period. In absence of such data and taking into account the calculated half-life, we estimate that at least 60% of the activity survived to the end of the irradiation. Thus the corrected number of the produced Eka-Hg is

$$N_0 \approx 1941$$

3. Production of Spallation Residues in Interaction of 24 GeV Protons with Tungsten Target

It is assumed that the production of element 112 in a W-target irradiated with 24 GeV protons is possible via fusion of Sr isotopes (spallation products) with W nuclei of the target. Marinov *et al.* [3] and Kolb *et al.* [17] suggest
$^{88}_{38}\mathrm{Sr} + {}^{184}_{74}\mathrm{W} \rightarrow {}^{272}_{112}\mathrm{Cn}$ and $^{86}_{38}\mathrm{Sr} + {}^{186}_{74}\mathrm{W} \rightarrow {}^{272}_{112}\mathrm{Cn}$ reactions.

We used HTAPE card in the MCNPX 2.7 code [18] to calculate the types and numbers of residual nuclei produced in the interaction of 24 GeV protons with a ^{nat}W-target. The target specifications were same as given by [1], *i.e.* cylindrical ^{nat}W targets of thickness (length) 120 g·cm^{-2} and mass of 33 g, which translates to a cylinder of diameter 0.6 cm and length 6.2 cm. In the calculations the direction of the proton beam coincided with the target axis.

Figure 1(a) shows the charge distribution of all isotopes (spallation products) and **Figure 1(b)** illustrates the yield of Sr isotopes (Z = 38) produced in the interactions. All together sixteen isotopes of Sr with (A = 77 to 92) with total yield of 8.32×10^{-3} per proton are produced. The spallation residue yield is strongly dependent on the target length (along the beam line); for a shorter target length it will be less than the above given figure.

From **Figure 1(b)** it is evident that most abundantly produced isotopes of Sr (62%) are those with mass numbers of 82, 83 and 84. Fusion of these isotopes with ^{184}W and ^{186}W will result in

$$^{82}_{38}\mathrm{Sr} + {}^{184}_{74}\mathrm{W} \rightarrow {}^{266}_{112}\mathrm{Cn} \quad \text{and} \quad {}^{82}_{38}\mathrm{Sr} + {}^{186}_{74}\mathrm{W} \rightarrow {}^{268}_{112}\mathrm{Cn}$$

$$^{83}_{38}\mathrm{Sr} + {}^{184}_{74}\mathrm{W} \rightarrow {}^{267}_{112}\mathrm{Cn} \quad \text{and} \quad {}^{83}_{38}\mathrm{Sr} + {}^{186}_{74}\mathrm{W} \rightarrow {}^{269}_{112}\mathrm{Cn}$$

$$^{84}_{38}\mathrm{Sr} + {}^{184}_{74}\mathrm{W} \rightarrow {}^{268}_{112}\mathrm{Cn} \quad \text{and} \quad {}^{84}_{38}\mathrm{Sr} + {}^{186}_{74}\mathrm{W} \rightarrow {}^{270}_{112}\mathrm{Cn}$$

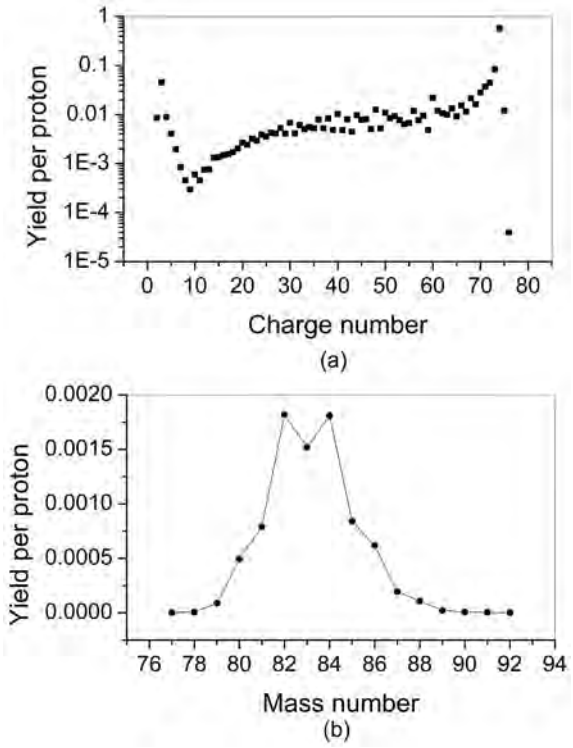

Figure 1. Spallation residues produced in 24 GeV p + ^{nat}W interactions. (a) Yield of all spallation products (b) Yield of Sr isotopes. Lines connecting data points are to guide the eye.

The mass numbers of Eka-Hg in the above given interactions are less than 272 given by Marinov *et al.* [3] and the products are neutron deficient isotopes.

Combined production rate of these three Sr isotopes ($^{82\text{-}84}$Sr) is 5.15×10^{-3} per proton which is 7 times higher than the combined production rates of ^{88}Sr and ^{86}Sr (7.25×10^{-4}), considered by Marinov *et al.* to be the principal participants in the fusion reaction with W nuclei [3].

4. Estimation of the Eka-Hg Production Cross-Section

An accurate estimation of the production cross-section of Eka-Hg with the available data is not possible for the following reasons:

1) The exact number of protons that hit the target is not known. From the publications it is not clear how the targets were irradiated? What was the proton direction with respect to the target axis? How was the beam fluence measured? Do the given proton numbers refer to those that hit the target or are they the numbers of the protons that were extracted from the accelerator?

Lack of this information in the publications implies that measurement of the production cross-section of Eka-Hg was not part of the experimental plan of Marinov *et al.*

2) As already mentioned, 16 isotopes of Sr are produced with different production rates. Out of these ^{88}Sr and ^{86}Sr have been nominated to produce ^{272}Cn via fusion with W nuclei. Each Sr isotope has its own fusion reaction cross-section with

a given W-isotope of ^{nat}W.

However a rough estimation of the production cross-section of ^{272}Cn is possible with the following assumptions:

1) The given proton numbers are actually those that hit the target.

2) The beam direction was along the target axis.

3) Cross-sections for $^{88}_{38}Sr + ^{184}_{74}W \rightarrow ^{272}_{112}Cn$ and $^{86}_{38}Sr + ^{186}_{74}W \rightarrow ^{272}_{112}Cn$ reactions are similar to each other.

Then, using the calculated yields of the Sr isotopes of the interest, isotope fractions of the W-isotopes in ^{nat}W and a beam dose of 7×10^{17} protons, one obtains a production cross-section of 1.6 nb.

5. Case of Uranium Target

Production of element 112 is possible via fusion of ^{238}U with Ca. Similar to the case of the W-target, we calculated the spallation residue yields in the interaction of 24 GeV protons with a U-target, of the same shape and dimensions as the W-target. The mass of U-target will be slightly less (~1.5%) than that of the W because of the difference in densities.

Figure 2(a) shows the charge distribution of all spallation residues produced in the interactions. Obviously the hump in the middle of the distribution is populated mainly with the ^{238}U-fission products.

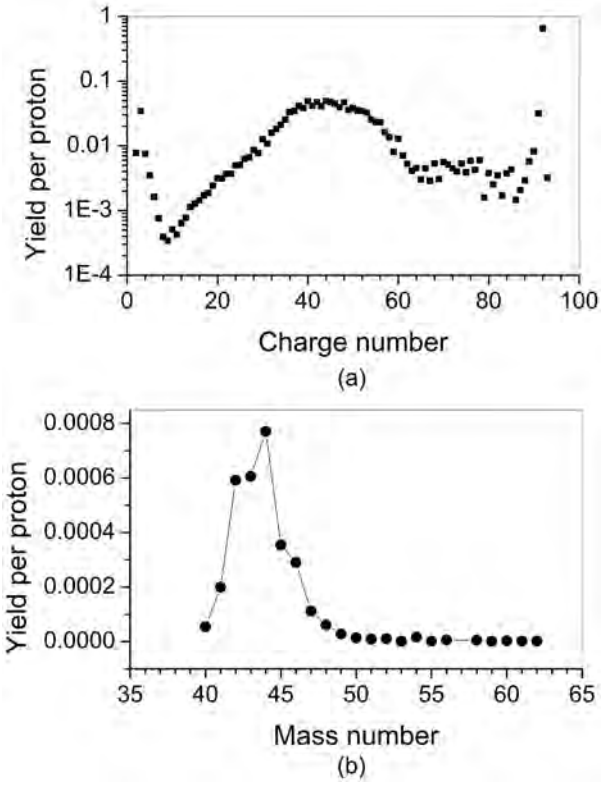

Figure 2. Spallation residues produced in 24 GeV p + ^{238}U interactions. (a) Yield of all spallation products; (b) Yield of Ca isotopes. Lines connecting data points are to guide the eye.

All together 22 isotopes of Ca with A = 40 - 62 are produced, with a total yield of 3.14×10^{-3} per proton. This is about 2.7 times less than the yield of Sr-isotopes produced in the W-target. Isotopes ^{42,43,44}Ca make about 63% of the total Ca yield. The yield of ^{48}Ca relevant to the experiments of Oganessian *et al.* [4] is less than 2% of the total Ca yield.

If isotopes ^{286}Cn and ^{283}Cn were produced in the proton irradiated U-target, they would not be detectable by chemical separation method because of their very short half-lives. If fusion of Ca isotopes (from the spallation residues) with ^{238}U nuclei in the target was possible then in order to produce the isotope ^{272}Cn, the post fusion compound nuclei must evaporate between 6 and 28 neutrons which is highly improbable for energetic reasons.

Boos *et al.* [19] irradiated a uranium target of mass 65 g with $(4 \pm 1) \times 10^{17}$ protons of 24 GeV using the CERN PS accelerator. The irradiation period was 20 days and chemical separation process of the target started three weeks after the end of the irradiation. They prepared two thin sources of HgS as carrier for Eka-Hg. For detection of the possible spontaneous fission activity in the HgS sources mica foils were placed in close contact with source 1 and 2 for periods of 2.6 y and 0.6 y, respectively. The mica foil placements on source 1 and 2 started 2.4 month and 1.4 month after the end of the irradiation, respectively. After exposure the mica foils were etched and scanned under an optical microscope; not a single fission track was detected.

The theoretical calculations given in this section confirm the experimental observations of Boos *et al.* [19].

6. Energy Distribution of the Spallation Products

Figure 3 shows the energy distribution of the all residual nuclei in the target volume, produced in interaction of the 24 GeV protons with ^{nat}W-target. As can be seen, almost all of the residual nuclei, regardless of their charge and mass have energies less than 100 MeV, well below (about one third of) the coulomb barrier

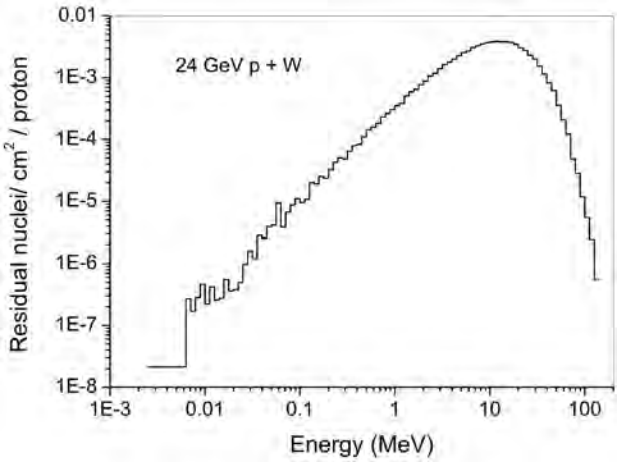

Figure 3. Energy distribution of the spallation residues produced in the interaction of 24 GeV protons with tungsten target of thickness 120 g·cm^{-2} and total mass of 33 g.

height of the (Sr + W) system. Therefore, if fusion of these nuclei in proton irradiated W-target were possible, then it had to be deeply sub-barrier fusion.

7. Effects of Proton Beam Energy on the Energy Distribution of Spallation Residues

Figure 4 shows the spectra of the neutrons and protons in interaction of 24 GeV protons with a tungsten target of thickness 120 g·cm^{-2} and mass 33 g. On average for every incident proton, there are 0.71 protons with energy greater than 23.7 GeV in the exit channel. Neutrons carry 5.2% and protons 80.6% of the beam energy. With energy and target size [1] used in the calculations majority of the beam protons leave the target without being engaged in an inelastic nuclear interactions and only lose small fraction of their energy via electronic interactions.

To increase the production rate of Sr nuclei in the W-target one need to:

1) Increase the target length to reduce number of the non-interacting beam protons.

2) Increase the beam dose at optimum proton energy.

Figure 5 shows the energy distribution of the heavy spallation residue (Z > 2) at different incident proton energies in interaction with a tungsten target of length 20 cm and diameter 0.6 cm. The energies of the spallation residue correspond to those at the moment of their production (*i.e.* maximum possible energy) and the energy degradation in the target environment is not taken into account. We chose a target with small diameter to reduce the amount of the unnecessary and disruptive radioactivity production. Obviously for a target of diameter 0.6 cm one prefers to have a proton beam of diameter less than 0.6 cm.

Spectra of the heavy ion residue at beam energies in the range of 3 GeV < $E_p \leq$ 24 GeV do not change significantly. For clarity of the figure in Figure 5 only the spectra at E_p > 5 GeV are shown. Most important, the total number of the produced ions per incident proton at different beam energies remains almost constant (Table 3). This is expected because; the heavy spallation residue mainly result from the proton induced fission of the target tungsten nuclei, a process that takes place after the cascade, pre-equilibrium and evaporation stages of the spallation reaction.

Table 3. Total number of heavy spallation residues produced on irradiation of a 20 cm long W target with protons of different energies.

Proton energy (GeV)	Total number of heavy ion residue per proton	Statistical uncertainty
0.5	2.5500E−02	1.10E−04
1	2.4400E−02	1.07E−04
5	2.5400E−02	1.14E−04
10	2.2200E−02	9.56E−05
15	2.2500E−02	9.69E−05
20	2.2900E−02	1.01E−04
24	2.3100E−02	1.02E−04

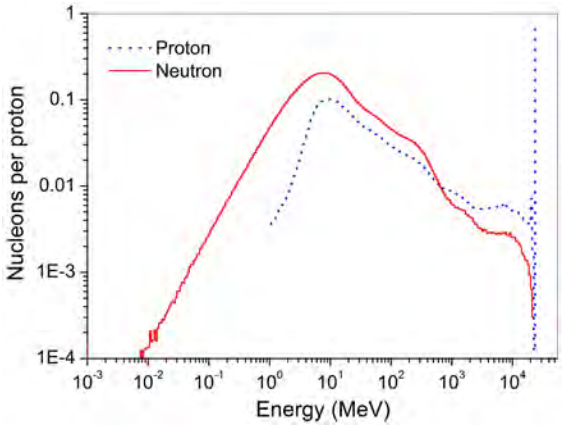

Figure 4. Spectra of the neutrons and protons escape the W-target (diameter 0.6 and length 6.2 cm) on its irradiation with 24 GeV protons.

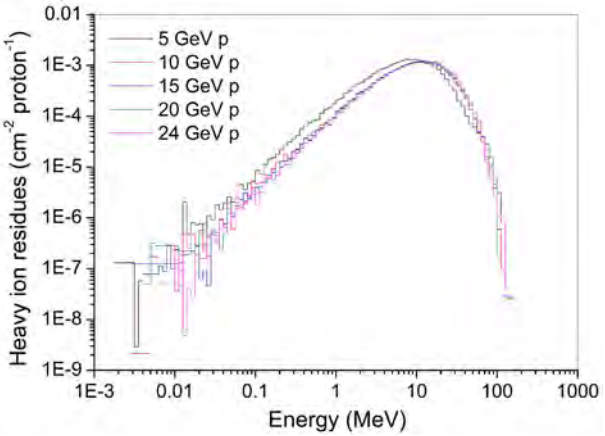

Figure 5. Energy distribution of the heavy nuclei (Z > 2) in irradiation of a W-target of diameter 0.6 cm and length 20 cm with protons of different energies.

Thus we conclude that if one intends to search for the interaction of any heavy spallation residue with the target nuclei, very high energy proton beam is not required.

8. Discussion

From the available published data [1] the half-life of the spontaneous fission events detected in the source from W2 target was estimated to be ~74 days.

Monte Carlo calculations show that, in the irradiation of a tungsten target with 24 GeV protons 16 isotopes of Sr are produced. The yields of these isotopes are sufficiently high to justify the assumption of the fusion reaction of Sr + W in the target. However, because of low energies of the spallation residues, if fusion of Sr and W nuclei in proton irradiated W-target were possible, then it had to be deeply sub-barrier fusion.

If sub-barrier fusion of (U + Ca) system is possible, auranium target irradiated with 24 GeV protons is not expected to showany isotopes of element 112. Most abundantly produced Ca isotopes are ^{42,43,44,45}Ca where the product mass range

goes from ^{40}Ca to ^{62}Ca. The post fusion compound nuclei need to evaporate 6 to 28 neutrons to reach mass 272 which is very unlikely. Short lived isotopes of element 112 produced via irradiation of ^{238}U with Ca ions will not be detectable because of the required long chemical separation and sample preparation times.

The proton dose of the W1 target was 2×10^{18} over an irradiation period of about one year. Similar to the case of the W2 target, it is estimated that the actual irradiation period during which the W1 target was receiving protons, was about 58 days. The estimated half-life and duration of the proton irradiation of the W1 target and considering that fission track recording started ~200 days after the end of the irradiation, failure to detect any spontaneous fission activity in source prepared from W1-target may therefore be justified.

Monte Carlo calculations using the MCNPX code show that energy distribution of the heavy ion spallation residue do not change for a very wide range of the incident proton energies. Therefore, if Sr + W fusion in proton irradiated W-target is possible, then one does not need to have very high energy proton beam. A relatively long target at a proton energy of ≥3 GeV will be sufficient to produce the desired number of Sr nuclei in the tungsten target.

9. Conclusions

Findings of Marinov *et al.* imply the following possibilities:

1) Production of super-heavy element in proton irradiated tungsten target.

2) Production of very long-lived isotope of SHE which are not known so far.

3) Production of SHE in deep sub-barrier fusion reactions.

4) Production of SHE with much higher cross-sections than those known so far.

We believe that new experiments with today's knowledge, experimental facilities and techniques are required to examine and test the reproducibility or otherwise disprove the Marinov *et al.* claims.

As strontium isotopes in the proton irradiated W-target will not have energies greater than 100 MeV (fission fragment energy), the most straightforward method for examining the Z = 112 production in a W-target is to irradiate a thin foil of W with a very heavy dose of 100 MeV Sr ions and look for fission events.

Conflicts of Interest

The authors declare no conflicts of interest regarding the publication of this paper.

References

[1] Marinov, A., Batty, C.J., Kilvington, A.I., Newton, G.W.A., Robinson, V.J. and Hemingway, J.D. (1971) Evidence for the Possible Existence of a Superheavy Element with Atomic Number 112. *Nature*, **229**, 464-467. https://doi.org/10.1038/229464a0

[2] Marinov, A., Batty, C.J., Kilvington, A.I., Weil, J.L., Friedman, A.M., Newton, G.W.A., Robinson, V.J., Hemingway, J.D. and Mather, D.S. (1971) Spontaneous Fission Previously Observed in a Mercury Source. *Nature*, **234**, 212-215.

https://doi.org/10.1038/234212b0

[3] Marinov, A., Eshhar, S., Weil, J.L. and Kolb, D. (1984) Consistent Interpretation of the Secondary-Reaction Experiments in W Targets and Prospects for Production of Superheavy Elements in Ordinary Heavy-Ion Reactions. *Physical Review Letters*, **52**, 2209-2212. https://doi.org/10.1103/PhysRevLett.52.2209

[4] Oganessian, Y.T., Yeremin, A.V., Popeko, A.G., Bogomolov, S.L., Buklanov, G.V., Chelnokov, M.L., Chepigin, V.I., Gikal, B.N., Gorshkov, V.A., Gulbekian, G.G., Itkis, M.G., Kabachenko, A.P., Lavrentev, A.Y., Malyshev, O.N., Rohac, J., Sagaidak, R.N., Hofmann, S., Saro, S., Giardina, G. and Morita, K. (1999) Synthesis of Nuclei of the Superheavy Element 114 in Reactions Induced by ^{48}Ca. *Nature*, **400**, 242-245. https://doi.org/10.1038/22281

[5] Oganessian, Y.T., Yeremin, A.V., Gulbekian, G.G., Bogomolov, S.L., Chepigin, V.I., Gikal, B.N., Gorshkov, V.A., Itkis, M.G., Kabachenko, A.P., Kutner, V.B., Lavrentev, A.Y., Malyshev, O.N., Popeko, A.G., Roháč, J., Sagaidak, R.N., Hofmann, S., Münzenberg, G., Veselsky, M., Saro, S., Iwasa, N. and Morita, K. (1999) Search for New Isotopes of Element 112 by Irradiation of ^{238}U with ^{48}Ca. *The European Physical Journal A—Hadrons and Nuclei*, **5**, 63-68. https://doi.org/10.1007/s100500050257

[6] Hofmann, S., Ninov, V., Heßberger, F.P., Armbruster, P., Folger, V, Münzenberg, G., Schött, H.J., Popeko, A.G., Yeremin, A.V., Saro, S., Janik, R. and Leino, M. (1996) The New Element 112. *Zeitschrift für Physik A Hadrons and Nuclei*, **354**, 229-230. https://doi.org/10.1007/s002180050036

[7] Esterlund, R.A., Stehney, A.F. and Steinberg, E.P. (1972) Secondary Nuclear Interactions of 11.5 GeV Protons on Uranium: A Search for Production of Transcurium Actinide Elements. *Nuclear Physics A*, **179**, 645-656. https://doi.org/10.1016/0375-9474(72)90609-4

[8] Katcoff, S. and Perlman, M.L. (1971) Experiments Related to Possible Production of Superheavy Elements by Proton Irradiation. *Nature*, **231**, 522-524. https://doi.org/10.1038/231522a0

[9] Unik, J.P., Horwitz, E.P., Wolf, K.L., Ahmad, I., Fried, S., Cohen, D., Fields, P.R., Bloomquist, C.A.A. and Henderson, D.J. (1972) Production of Actinides and Search for Super-Heavy Elements Using Secondary Reactions Induced by GeV Protons. *Nuclear Physics A*, **191**, 233-244. https://doi.org/10.1016/0375-9474(72)90513-1

[10] Westgaard, L., Erdal, B.R., Hansen, P.G., Kugler, E., Sletten, G., Sundell, S., Fritsch, T., Henrich, E., Theis, W., Wolf, G.K., Camplan, J., Klapisch, R., Meunie, R., Poskanzer, A.M., Stephan, C. and Tys, J. (1972) Search for Super-Heavy Elements produced by Secondary Reactions in Uranium. *Nuclear Physics A*, **192**, 517-523. https://doi.org/10.1016/0375-9474(72)90088-7

[11] Barber, R.C., Gäggeler, H.W., Karol, P.J., Nakahara, H., Verdaci, E. and Vogt, E. (2009) Discovery of the Element with Atomic Number 112 (IUPAC Technical Report). *Pure and Applied Chemistry*, **81**, 1331-1343. https://doi.org/10.1351/PAC-REP-08-03-05

[12] Brandt, R., Ditlov, V., Firu, E., Ganssauge, E., Haiduc, M., Hashemi-Nezhad, R., Neagu, A.T. and Westmeier, W. (2018) Comment on the Recent Start of a New "IUPAC-Project". *World Journal of Nuclear Science and Technology*, **8**, 121-127. https://doi.org/10.4236/wjnst.2018.83010

[13] Malykhin, A.P., Yaroshevich, O.I., Levadni, V.A. and Roginetc, L.P. (1970) Measurement of Fission Density Distributions on Critical Facilities. *Vestsi Akademii Navuk Belarusi, Seryya Fizika-Energetychnykh Navuk*, **2**, 16-20.

[14] Hashemi-Nezhad, S.R., Zhuk, I., Potapenko, A.S. and Krivopustov, M.I. (2006) Calibration of Track Detectors for Fission Rate Determination: An Experimental and Theoretical Study. *Nuclear Instruments and Methods in Physics Research Section A*, **568**, 816-825. https://doi.org/10.1016/j.nima.2006.08.044

[15] Gilardoni, S. and Manglunki, D. (2011) Fifty Years of the CERN Proton Synchrotron. CERN-2011-004, CERN, Geneva.

[16] Shaw, E.N. (1971) CERN: A European Enterprise. *Europhysics News*, **2**, 3-6. https://doi.org/10.1051/epn/19710203003

[17] Kolb, D., Marinov, A., Newton, G.W.A. and Brandt, R. (2004) The Chemical Separation of Eka-Hg from CERN W Targets in View of Recent Relativistic Calculations. arXiv:nucl-ex/0412010.

[18] Pelowitz, D.B. (2011) MCNPX User's Manual, Version 2.7.0. LA-CP-11-00438, Los Alamos National Laboratory.

[19] Boos, A.H., Brandt, R., Molzahn, D., Patzelt, P., Vater, P., Bächmann, K. and Ross, E. (1976) Continued Search for Superheavy Elements Produced by Secondary Reactions of 24 GeV Protons Onuranium. *Radiochemical and Radioanalytical Letters*, **25**, 357-364.

World Journal of Nuclear Science and Technology, 2018, 8, 160-175
http://www.scirp.org/journal/wjnst
ISSN Online: 2161-6809
ISSN Print: 2161-6795

Prediction of Neutronic and Kinetic Parameters of Ghana Research Reactor 1 (GHARR-1) after 19 Years of Operation Using Monte Carlo-N Particle (MCNP) Code

Bright Madinka Mweetwa[1], Emmanuel Ampomah-Amoako[2], Edward Horga Kordzo Akaho[2], Cecil Odoi[2]

[1]National Institute for Scientific and Industrial Research, Lusaka, Zambia
[2]School of Nuclear and Allied Sciences, University of Ghana, Accra, Ghana
Email: bmbright2@yahoo.co.uk

How to cite this paper: Mweetwa, B.M., Ampomah-Amoako, E., Akaho, E.H.K. and Odoi, C. (2018) Prediction of Neutronic and Kinetic Parameters of Ghana Research Reactor 1 (GHARR-1) after 19 Years of Operation Using Monte Carlo-N Particle (MCNP) Code. *World Journal of Nuclear Science and Technology*, **8**, 160-175.
https://doi.org/10.4236/wjnst.2018.84014

Received: August 11, 2018
Accepted: October 12, 2018
Published: October 15, 2018

Abstract

The Ghana Research Reactor-1 (GHARR-1) core was modified with an addition of a 9.0 mm layer of beryllium to the top shim tray to compensate for reactivity loss due to fuel depletion after 19 years of operation. Neutronic and kinetic parameters have been predicted using Monte Carlo N-Particle Code version 5 (MCNP5) to determine whether they were within acceptable operating margins. Excess reactivity, control rod worth, moderator reactivity coefficient, delayed neutron fraction and neutron generation time have been predicted as 3.86, 6.98, −0.1218 mk/°C, 8.17507×10^{-3} $\Delta k/k$, and 8.147×10^{-5} s respectively. These parameters compared favorably with those provided in the initial Safety Analysis Report.

Keywords

Delayed Neutron Fraction, Neutron Generation Time, Moderator Reactivity Coefficient, Power Peaking Factor

1. Introduction

The Ghana Research Reactor-1 (GHARR-1) has undergone core conversion from the use of 90.2% high enriched uranium (HEU) fuel to the use of 12.5% low enriched uranium (LEU) fuel. The conversion of the reactor core was done under a project supported by the International Atomic Energy Agency (IAEA) with the aim of reducing proliferation risks associated with HEU fuel [1]. Con-

version of the core was of benefit to Ghana Atomic Energy Commission (GAEC), as the reactor core had been in operation for 19 years.

During the 19 years of operation, the excess reactivity of the HEU core dropped from 4.0 mk to about 2.3 mk due to fuel depletion and accumulation of fission products, some of which are neutron poisons. To restore the excess reactivity to the required 4.0 mk, the HEU core was modified with an addition of 9.0 mm of beryllium to the top shim tray. This modification was supported by an assessment of various safety parameters [2]. The assessment of safety parameters and associated operational margins was necessary to provide an indication of whether the reactor would operate safely in all modes. Besides assessment of the safety parameters, it was also necessary to document the operating conditions of the HEU core after addition of beryllium to the top shim tray as well as to update the final safety analysis report (SAR) related to conversion of core as required by the regulatory authority. Data generated under this work will also be used as reference for operating conditions of the LEU cores since it was envisaged that the operating conditions of the LEU would be similar to those of the HEU [3].

The safety parameters that were updated in the final SAR for the HEU core are; thermal hydraulics, neutronics and kinetics respectively. Thermal hydraulic parameters are not discussed under this work but have been discussed in [2]. This work assesses neutronic and kinetic parameters of GHARR-1's HEU core after 19 years of operation and subject to addition of 9.0 mm of beryllium to the top ship tray.

Description GHARR-1

The reactor was designed by the China Institute of Atomic Energy (CIAE) and was commissioned in 1986. It was designed to operate with a nominal power of 30 kW and a maximum neutron flux of 1×10^{12} n/cm^2·s. The core was designed to use HEU as fuel, beryllium as reflector, light water as a moderator as well as a coolant and natural convection for cooling. The reactor was used for educational purposes, human resource development in nuclear science and technology, neutron activation analysis, and production of short-lived radioisotopes for use in hospitals. The core had 354 lattice positions arranged in 10 concentric circles at a pitch distance of 10.95 mm. It had 344 uranium-aluminum (U-Al) alloy fuel elements, 6 dummy aluminium elements, 4 tie rods, 2 grid plates and a central guide tube for the cadmium control rod. It was surrounded by an annular beryllium reflector and rested on a block of beryllium reflector plate. The top part of the core had a shim tray which was used for adding layers of beryllium for increased neutron reflection and reactivity insertion into the core. The top shim tray design allowed for reactivity compensation due to fuel depletion and accumulation of fission products as the reactor operated. **Figure 1** shows a schematic diagram of the vertical cross-section of GHARR-1's HEU core.

The reactor was under moderated with a high negative moderator temperature reactivity coefficient (approximately −0.l mk/˚C for the temperature range

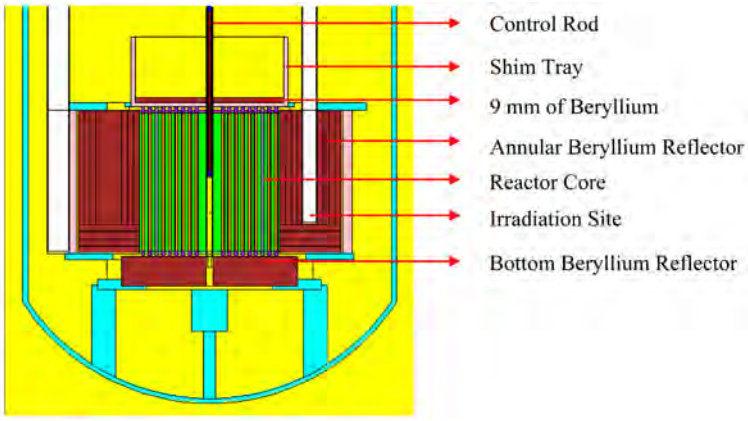

Figure 1. A schematic diagram of the vertical cross-section of GHARR-1 [1].

20˚C - 45˚C), and a low critical mass which rendered it inherently safe. The availability of these characteristics, assured safety of the reactor under an array of possible accident conditions, such as power excursion that would occur following an accidental insertion of reactivity into the core [4] [5].

2. Theory

Neutron interactions with reactor materials cause different phenomena such as nuclear fission, induced radioactivity and associated decay heating. These interactions play a central role in creating the power distributions, within nuclear materials, that drive the heat transfer process in a reactor. They also help in the determination of reactor safety, core properties, reactivity control, reactor kinetics, xenon stability, fuel depletion, and are also important for isotope production [6]. Reactor properties can deviate from nominal conditions due to planned or unplanned changes in reactivity and abnormal or accident conditions. The deviation from nominal conditions has an effect on the neutron flux in the reactor core.

An understanding of the time-dependent behavior of neutrons in a nuclear reactor is important in the analysis of nuclear reactor safety. The transient neutron flux behaviour resulting from a departure from criticality may arise during operational changes such as control rods movement, environmental changes such as those of boron concentration, or accidental disturbances in steady-state operating condition. This phenomenon, among others, may be classified as either reactor kinetics or reactor dynamics.

Reactor kinetics also known as reactor kinetics without feedback, is the study of the neutron flux's time-dependence for postulated changes in the macroscopic cross sections. Reactor dynamics or reactor kinetics with feedback and with spatial effects, is the study of the time-dependence of a neutron flux on the macroscopic cross sections as a function of the neutron flux level [7]. The kinetic parameters of importance in safety evaluation of a nuclear reactor are the effective delayed neutron fraction, prompt neutron lifetime and neutron generation time [8].

Neutronics of a nuclear reactor is the study of the distribution and multiplication of neutrons in the reactor and its effect on reactor power distribution. Diffusion codes are important in the study of neutronics and also in the determination of the neutron flux from the solution of the neutron diffusion equation. The neutron flux is important in computing the power distribution [9]. It also looks at how neutrons multiply in a reactor. The neutronic parameters that are important for the dynamic reactor behaviour are the excess reactivity, shutdown margin, control rod worth, power peaking factors and the various reactivity coefficients [10].

The multiplication of neutronsis is important if a reactor has to sustain a chain reaction. In order to have a sustainable chain reaction, neutrons emitted during fission should be able to cause further fissions in other fissile or fissionable nuclei. The fission chain reaction is quantitatively expressed in terms of the effective neutron multiplication factor (K_{eff}). The neutron multiplication factor, expressed by Equation (1), is a ratio of the number of neutrons in the current generation and the number of neutrons in the preceding generation. This factor is dependent on various parameters that also vary with temperature and are linked to reactor safety.

$$k_{eff} = \frac{\text{Number of neutrons in one generation}}{\text{Number of neutrons in the preceding generation}} \tag{1}$$

When K_{eff} is equal to unit, the reactor is said to be critical, when above or below unit, the reactor is said to be super critical or subcritical respectively. The measure of a reactor's departure from criticality is called reactivity (ρ) and is defined as a fractional change in neutron population per generation. Equation (2) shows the mathematical expression of reactivity.

$$\rho = \frac{k_{eff} - 1}{k_{eff}} \tag{2}$$

The ability to predict correctly the effective multiplication factor (K_{eff}) and computation of reactivity (ρ) is fundamental to solutions of criticality problems. The K_{eff} and ρ are important in the computation of such parameters as; the delayed neutron fraction, control rod worth, shutdown margin, neutron life time, and neutron generation time (Λ).

Correct computation of the prompt neutron generation time for a nuclear reactor under design or whose configuration has been modified is important for prediction and optimization of various reactor parameters. The neutron generation time has a bearing on various interactions and environmental conditions within a reactor. The prompt neutron generation time (Λ) is the average time from birth of a neutron to a point it reproduces itself through fission. The prompt neutron generation time can also be defined as the inverse of the neutron production rate as expressed by Equation (3). This is applicable when considering a one-group diffusion-theory approximation.

$$\Lambda = \frac{1}{Vv\Sigma_f} \tag{3}$$

where V in the average neutron velocity, ν is the average number of neutrons produced per fission and Σ_f in the fission macroscopic cross section.

There is, however, a difference between neutron generation time and neutron life time. Neutron life time is the time period between the birth of a neutron and its absorption. The neutron life time can be used to determine the neutron generation time using Equation (3). In light water reactors, the prompt neutron generation time increases with fuel burn up. This may be caused by a reduction in fissile materials as well as absorption in the moderator which makes the prompt neutron live much longer [11].

One of the commonly used method for determining the neutron generation time is the $1/V$ absorber method. This method applies the K_{eff} and ρ to compute the neutron generation time. In this method, all reactor materials in the core model are doped with small amounts of a $1/V$ neutron absorber material. The $1/V$ neutron absorber material inserts a negative reactivity expressed by Equation (4).

$$\rho = -\frac{\Delta k}{k} = \frac{k_u - k_{pt}}{k_u * k_{pt}} \tag{4}$$

where K_{pt} is the perturbed multiplication factor due to the $1/V$ neutron absorber material and K_u is the steady state unperturbed multiplication factor. According to Bretscher [12] [13] the negative reactivity inserted is equal to the product of the neutron lifetime (l_p), the atomic density (n) of the $1/V$ neutron absorber material (atoms/b-cm), the speed of thermal neutrons (V = 2.2E5 cm/s), and the absorption cross section (σ = 3837b) of the $1/V$ neutron absorber material. This relation is expressed by Equation (5).

$$-\frac{\Delta k}{k} = l_p V n \sigma \quad \text{thus} \quad l_p = \frac{-\frac{\Delta k}{k}}{V n \sigma} \tag{5}$$

The neutron generation time is given as the limit of l_p as the n approaches zero. Equation (6) gives the expression for the neutron generation time.

$$\Lambda = \lim_{n \to 0} l_p = \lim_{n \to 0} \frac{-\frac{\Delta k}{k}}{V n \sigma} \tag{6}$$

3. Method and Materials

Monte Carlo N-Particle Transport (MCNP) is a general-purpose, continuous-energy, generalized-geometry, time-dependent, coupled neutron/photon/ electron Monte Carlo Transport code. The MCNP code is useful for complex problems that cannot be modeled by computer codes that use deterministic methods. Various cases can be simulated in several transport modes: neutron only, photon only, electron only, combined neutron/photon transport where the photons are produced by neutron interactions, neutron/photon/electron, photon/electron, or electron/photon. The neutron energy regime is from 10^{-11} MeV to 20 MeV, and the photon and electron energy regimes are from 1 keV to 1000 MeV. The capa-

bility to calculate K_{eff} eigenvalues for fissile systems is also a standard feature. The individual probabilistic events that comprise a process are simulated sequentially. The probability distributions governing these events are statistically sampled to describe the total phenomenon. It consists of following each of the many particles from a source throughout its life to its death in some terminal category (absorption, escape, etc.). Probability distributions are randomly sampled using transport data to determine the outcome at each step of its life. In this work, MCNP was used because of its ability to model complex three-dimensional geometries and its extensive validation [14].

3.1. Modification to GHARR-1's MCNP Model

The Reactor Burn up System (REBUS) code has been used to generate an inventory of isotopes produced due to fission products and fuel burn up after 19 years of GHARR-1's operation. The REBUS code was simulated under GHARR-1's operation scheme of 2.5 hours per day, 4 days a week and 52 weeks a year. This was done to produce an inventory of isotopes that was reflective of GHARR-1's operating period. This inventory of isotopes was used to update the material card's fuel composition in GHARR-1's MCNP5 model. The material card is used to define the composition of different materials in the reactor model. A 9.0 mm layer of beryllium was added to the top shim tray of the reactor core as can be seen in **Figure 1**. The addition of beryllium added a reactivity worth of 1.3 mk which was sufficient to compensate for reactivity loss in the core due to fuel burn up and accumulation of fission products after 19 years of operation.

3.2. MCNP Simulation Criticality Problem

Criticality problems in MCNP are simulated using the KCODE card which requires an input of the nominal number of source histories (N) per cycle, an initial guess of K_{eff}, the number of source cycles (I_c) to be skipped before K_{eff} can accumulate, the number of active cycles (I_A), and the total number of cycles (I_t) [15].

The control rod worth, delayed neutron fraction, neutron generation time, shutdown margin, and power peaking factor cases have been simulated with the following specifications in the model; N was set at 300,000, K_{eff} was given an initial guess of 1.004, I_t was set as 250 cycles with I_c set at 20 cycles and the remaining I_A set 230 cycles being active. These values were adequate to provide sufficient statistical accuracy in the results. The value for the number of cycles to be skipped was chosen to provide enough cycles for K_{eff} to statistically converge around a certain solution, allowing for the most accurate results to be obtained. The initial guess for K_{eff} of 1.004 was based on the K_{eff} for GHARR-1's clean core value, thus this value was sufficient to allow for good statistical accuracy in the prediction of K_{eff}. A total of 69 million particles were used for each simulation.

3.2.1. Excess Reactivity

Simulation for K_{eff} was performed with the control rod fully withdrawn and the

KCODE card parameters set as described in Section 3.1. The K_{eff} obtained was used to compute the excess reactivity using Equation (7).

$$\rho = \frac{k_{eff} - 1}{k_{eff}} \tag{7}$$

3.2.2. Shutdown Margin

The core has been simulated with the control rod fully inserted into the reactor core. The K_{effin} obtained has been used to compute ρ_{sdm} using Equation (8).

$$\rho_{sdm} = \frac{1 - k_{eff_{in}}}{k_{eff_{in}}} \tag{8}$$

3.2.3. Control Rod Worth

Two cases have been simulated to obtain the eigenvalues needed to compute the control rod worth. For the first case, the control rod was fully withdrawn, giving a multiplication factor K_{effout}, and in the second case, the control rod was fully inserted into the reactor core giving the multiplication factor K_{effin}. Equation (9) was used to compute the control rod worth (ρ_{crw}).

$$\rho_{crw} = \frac{k_{eff_{out}} - k_{eff_{in}}}{k_{eff_{out}} k_{eff_{in}}} = \rho_{out} - \rho_{in} \tag{9}$$

3.2.4. Reactivity Coefficients

Reactivity coefficients have been simulated with the following KCODE card input; N was set at 200,000, K_{eff} was given an initial guess of 1.004, I_t was set at 220 cycles with the first 20 cycles I_c being inactive and the 200 cycles I_A being active. A total of 40 million particle histories have been used.

3.2.5. Moderator Temperature Coefficient

To obtain multiplication factors required to determine the moderator temperature coefficient, changes were made to the TMP card and all Cell cards that contain water in the MCNP model for GHARR-1. The TMP data card allows for input of equilibrium energy (MeV) of atoms in the fuel at a particular temperature. The TMP card and all Cell cards containing water in the model were respectively updated with the equilibrium temperature (MeV) and density corresponding to the temperature (˚C) that was being simulated for. The multiplication factors were predicted for the temperature range 20˚C to 100˚C. **Table 1** shows the temperatures that have been used for predicting K_{eff} and their corresponding equilibrium temperatures, densities and percent voiding. Corresponding reactivities for the temperature ranges have been computed using Equation (8). Each moderator reactivity computed has been plotted against the corresponding temperature (˚C) to obtain the relationship between temperature (˚C) and reactivity. The reactivity response to change in temperature has been determined using the 2nd order differential equation. Equation (10) has been used to compute the moderator temperature coefficients.

Table 1. Relationship between temperature, equilibrium energy density and percent void.

Temperature (˚C)	Equilibrium energy (MeV)	Density (g/cm^3)	Void (%)
20	2.5125e−08	0.99820	0.00
30	2.6124e−08	0.99567	0.18
40	2.6935e−08	0.99221	0.70
50	2.7847e−08	0.98807	1.02
60	2.8709e−08	0.98324	1.50
70	2.9571e−08	0.97777	2.00
80	3.0432e−08	0.97170	2.55
100	3.2156e−08	0.95835	3.91

$$\alpha_x = \frac{\partial \rho}{\partial x} \tag{10}$$

where α_x is the reactivity coefficient for parameter (x).

3.2.6. Moderator Void Coefficient

The MCNP5 code does not have a card to input percent voiding in water due to changes in temperature. An indirect method has been used where densities corresponding to percent void as presented in Table 1 for the temperature range 20˚C to 100˚C were used. This indirect method is an accurate way for water voiding in MCNP Daniel [16]. The temperature range 20˚C to 100˚C was chosen to cover both normal and higher temperatures. During normal operations of the reactor, the coolant temperature does not change significantly, however higher temperatures were chosen to study the behaviour of the moderator void coefficient at higher temperature.

All Cell cards containing water and the TMP card were respectively updated with densities and corresponding temperatures (˚C) for the range 20˚C to 100˚C. Respective multiplication factors have been predicted for each temperature. Corresponding reactivities for the temperature range 20˚C to 100˚C were computed using Equation (8). Table 1 shows the densities and their relative percent voids and temperatures that were used. The relationship between temperature and reactivity was determined using the 4th order polynomial equation. Equation (10) was used to compute the moderator void coefficient.

3.2.7. Fuel Temperature Coefficient

The TMP data card was updated with temperatures for the range 30˚C to 600˚C. This range was adequate to cover the operating range for the U-Al alloy fuel whose melting temperature is 640˚C. It was also sufficient to give an indication of the variation of the fuel temperature coefficient under accident conditions. The multiplication factors were predicted for the temperature range 30˚C to 600˚C. Corresponding reactivities for the temperature range 30˚C to 600˚C were computed using Equation (8). The relationship between temperature and reactivity was determined using the 4th order polynomial equation. Equation (10)

was used to compute the fuel temperature coefficient.

3.3. Kinetic Parameters

3.3.1. Effective Delayed Neutron Fraction

The effective delayed neutron fraction (β_{eff}) has been determined using the Prompt method which requires prediction of the multiplication factor for two cases [17]. The first case involves prediction of the multiplication factor for prompt neutrons (K_p) only without the delayed neutrons. The second case involves prediction of the multiplication factor (K_{eff}) which combines both prompt and delayed neutrons.

In this method, the TOTNU data card with entry NO has been used to obtain the multiplication factor for prompt neutrons only. The TOTNU data card with entry NO prevents the influence of delayed neutrons on multiplicity per fission. Thus, the multiplicity per fission is due to the average prompt neutron and subsequently K_p is predicted for all fissionable nuclides with available prompt values.

The TOTNU card without any entry has been used to predict the average number of neutrons from fission. The TOTNU card without any entry considers both prompt and delayed neutrons and the resultant effective multiplication factor expressed by Equation (1) is given as K_{eff}.

For both cases, the KCODE card parameters were set as described in Section 3.1. The values for K_p and the K_{eff} have been used to compute the delayed neutron fraction using Equation (11).

$$\beta_{eff} = \frac{1-k_p}{k_{eff}} \tag{11}$$

3.3.2. Neutron Generation Time

The neutron generation time has been determined using the $1/V$ absorber method described in Section 2. Boron-10 has been used as a doping material because of its $1/V$ neutron absorption property. Eleven cases have been used to predict multiplication factors required for the determination of the neutron generation time (Λ). The first case was used to predict the unperturbed multiplication factor (K_u) an equivalent of the multiplication factor K_{eff} described by Equation (1) for a reactor without any doping materials added. The remaining 10 cases have been used to predict the perturbed multiplication factors (K_{pt}) for10 different concentrations of boron-10 in the range 6.0×10^{-8} - 15×10^{-8} atoms/b-cm. Concentrations of boron lower than 6×10^{-8} atoms/b-cm have not been used since they do not provide significant change in reactivity as it has been reported by Hanson A. L. and Diamond D. J. [18]. **Table 2** shows the concentrations of boron-10 that were used to dope reactor core materials. For each of the 11 cases, the KCODE card has been used to predict multiplication factors with parameters set as described in Section 3. The corresponding negative reactivity inserted and the prompt neutron lives were computed using Equations (4) and (5). The various neutron life time (l_p) obtained using Equation (5) have been

Table 2. Boron-10 concentrations for reactor core material perturbation.

Case	Boron-10 Concentration (atoms/b-cm)
1	Normal Condition
2	6.0×10^{-8}
3	7.0×10^{-8}
4	8.0×10^{-8}
5	9.0×10^{-8}
6	10.0×10^{-8}
7	11.0×10^{-8}
8	12.0×10^{-8}
9	13.0×10^{-8}
10	14.0×10^{-8}
11	15.0×10^{-8}

plotted against their corresponding boron concentrations. The neutron generation time (Λ) has been determined as the intercept on the Y-axis based on the graphical application of Equation (6).

4. Results and Discussion

Table 3 shows a comparison of neutronic and kinetic parameters from this work and those provided for in the initial GHARR-1 Safety Analysis Report. Neutronic parameters for GHARR-1 after 19 years of operation were observed to be in good agreement with those provided in the initial SAR. The excess reactivity was predicted to be within the expected margin of 3.5 mk to 4.0 mk and it was also determined to be less than the limiting value of $1/2\beta_{eff}$ as required if the reactor is to operate normally. If the excess reactivity exceeds $1/2\beta_{eff}$, the reactor would tend to prompt criticality with a power excursion within seconds rendering it impossible to control. The control rod worth was predicted to be slightly higher compared to the value reported in the SAR even though the two values were fairly in agreement. The higher value from this work could be attributed to the increased margin between reactivities ρ_{out} and ρ_{in} described by Equation (9). It is expected that the reactivity ρ_{in} inserted when the control rod is fully inserted into the reactor core would be lower for the core after 19 years of operation compared to the value provided in the initial SAR due to increased negative reactivity resulting from fuel depletion and accumulation of neutron poisons. This causes a wider margin between the two reactivities making the control rod worth slightly higher. The control rod worth is an important design parameter for the safety of a reactor.

The shutdown margin (ρ_{sdm}) was predicted to be slightly higher compared to the value provided in the initial SAR. This could be attributed to a reduced value of the multiplication factor K_{effin} for the control rod fully inserted into the reactor core. From Equation (8), the reduced K_{effin} implies an increased value of ρ_{sdm}.

Table 3. Comparison of neutronic and kinetic parameters from this work and the SAR.

Simulation Results	Irradiated Core	Sigma	Safety Analysis Report (SAR)
Control rod fully withdrawn	1.00388	1.4×10^{-4}	1.00400
Excess reactivity (mk)	3.86	-	4.0
Control rod fully inserted	0.99689	1.4×10^{-4}	-
Control rod worth	6.98	2.0×10^{-2}	6.8
Shutdown margin	3.12	8.0×10^{-2}	3.0
Delayed neutron fraction ($\Delta k/k$)	8.17507×10^{-3}	4.0×10^{-4}	8.08×10^{-3}
Neutron generation time ($\Delta k/k$)	8.147×10^{-5}	2.0×10^{-6}	8.12×10^{-5}
Maximum power peaking factor	1.3522	-	1.3525
Moderator reactivity coefficient (mk/˚C)	−0.1218	-	−0.1

The reduction in the value of multiplication factor K_{effin} compared to that in the SAR is influenced by increased neutron absorption due to accumulated neutron poisons in the fuel after 19 years. Despite the addition of a layer of beryllium to the top shim tray, the neutron poisons accumulated in the fuel still add a small amount of negative reactivity into the reactor core. This negative reactivity causes the ρ_{sdm} to be slightly higher compared to that reported in the SAR.

Figure 2 compares the axial power density distribution of the reactor core after 19 years and that of the core provided in the initial SAR. The axial power density distribution has its maximum value at the center of the core. This could be attributed to the presence of water as a moderator in the control rod guide tube when the control rod is fully withdrawn, and the presence of the annular beryllium reflector around the center that causes a dense population of neutrons due to low neutron leakage in the center compared to the top and bottom parts of the reactor core. As can be observed, the power density starts decreasing axially from the center of the core. However, towards the top shim tray and the bottom beryllium block, it starts increasing again. The increase in power density towards the top and bottom beryllium blocks is influenced by increased neutron population as a result of neutrons being reflected by beryllium.

Both power distributions for the core after 19 years and that of the core provided in the initial SAR tilt lower towards the top of the reactor core. This implies the power at the top of the core in both cases is lower compared to the bottom of the core. This could be attributed to high neutron leakage at the top of the core compared to the bottom parts of both cores. The top part of the initial core is bare and that of the core after 19 years is reflected by 9 mm of beryllium compared to 50 mm of beryllium for the bottom parts of both cores.

Both the core after 19 years and that provided in the initial SAR show a similar power density distribution. However, the distribution for the core after 19 years is lower compared to that of the core provided in the initial SAR for the bottom part of the power density distribution. The lowered power density distribution observed near the bottom for the core after 19 years compared to the

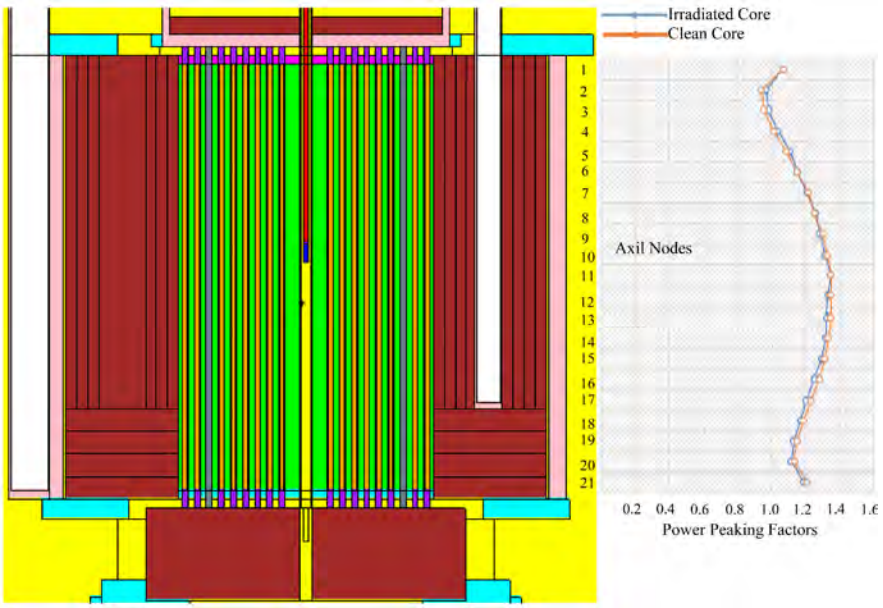

Figure 2. Comparison of axial power distribution of the ırradiated and clean cores.

core provided in the initial SAR could be attributed to accumulated fission products including neutron poisons in the fuel. These neutron poisons are not present in the core provided in the initial SAR. Towards the top of the core, there is an overlap where the core after 19 years has a higher power density distribution compared to the core provided in the initial SAR. The power density distribution overlap observed could be attributed to increased neutron density due to the presence of a 9.0 mm of beryllium that was added to the top shim tray after 19 years of operation.

The maximum power peaking factor for the core after 19 years was predicted to be 1.3522 and that of the core provided in the initial SAR was predicted to be 1.3525. Both values are within the expected range or 1.3 - 1.5 for light water moderated research reactors.

Figure 3 compares the integral control rod worth of the core after 19 years with that of the core provided in the initial SAR. The plot shows that the control rod worth for the core after 19 years is lower compared to that of the core provided in the initial SAR for the length 0.0 mm to 215.0 mm from the bottom of the core. Beyond 215.0 mm, the control rod worth for the core after 19 years is higher compared to that of the core provided in the initial SAR. The lower neutron population due to fuel depletion and presence of neutron poisons in the bottom part of the core after 19 years causes the control rod to absorb fewer neutrons. This is observed through the lower values of the control rod worth for the core after 19 years compared to that of the core provided in the initial SAR. The integral control rod is an important design feature which shows how efficient a control rod is in absorbing neutrons.

Figure 4 shows a plot of the neutron lifetime (l_p) against boron-10 concentration. The neutron generation time (Λ) was determined as the intercept on the

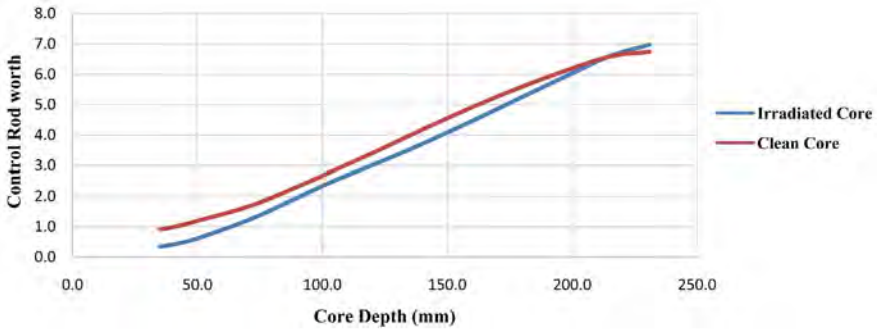

Figure 3. Comparison of the Integral control rod for the irradiated and clean cores.

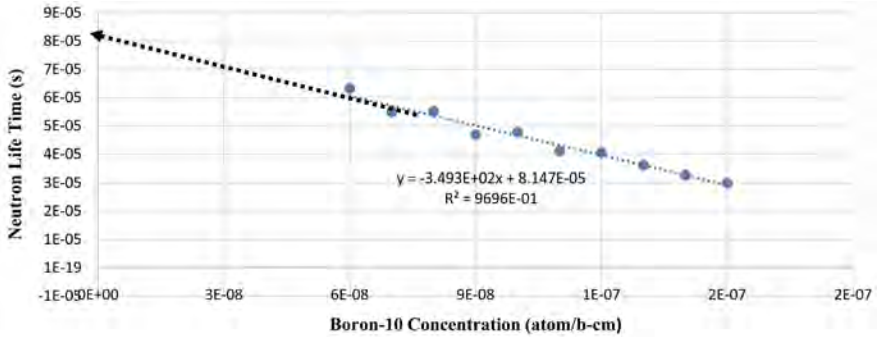

Figure 4. Plot of neutron life time against boron concentration.

neutron-lifetime axis. The mathematical computation is elaborated in Equations (3) to (6). The value for the neutron generation time for the core after 19 years of operation was determined to be slightly higher compared to that of the core provided in the initial SAR. This could be attribute, in part, to the reduced average number of neutrons produced per fission due to fuel depletion and accumulation of neutron poisons in the fuel despite the addition of 9.0 mm of beryllium to the top shim tray. In light water reactors, the prompt neutron generation time increases with fuel burnup. This may be caused by a reduction in fissile materials as well as absorption in the moderator which makes the prompt neutron live much longer. Mathematically, this could be explained using Equation (3) from which the variable is the number of neutrons produced per fission. Reduction of this value implies an increase in the prompt neutron generation time.

Moderator Void Coefficient

The moderator void coefficient for the temperature range 20˚C to 100˚C was predicted to be negative. **Figure 5** shows the relationship between water voiding and reactivity. The correlation between water voiding and reactivity was determined to be negatively strong with a value of −0.9839. This entails, an increase in water voiding due to an increase in temperature, would cause a decrease in reactivity. This is a safety design feature of the reactor which renders it safe in case of an accidental insertion of abnormal reactivity that could cause boiling and voiding. In case boiling occurred, the reactivity would reduce thus preventing power excursion. Equation (12) shows the moderator void coefficient as a

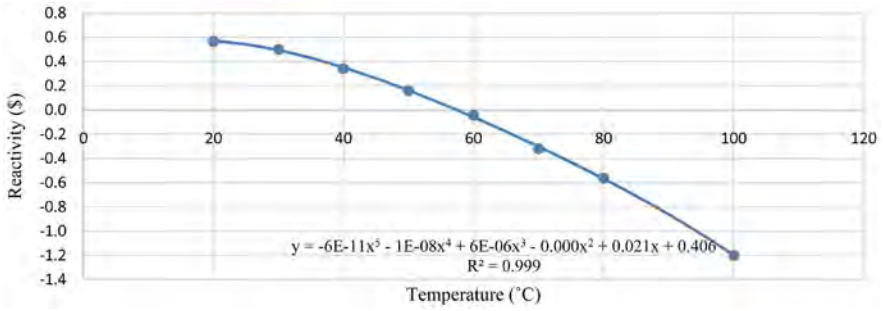

Figure 5. Moderator density (void) change with temperature (˚C).

function of temperature for the reactor core after 19 years of operation.

$$\alpha_v(T) = 3.0\times10^{-10}T^4 - 4\times10^{-8}T^3 + 1.8\times10^{-5}T^2 - 0.0016T + 0.021643 \quad (12)$$

It can be observed from **Table 4** and **Figure 5** that the temperature feedback becomes more negative for greater temperatures of water. Thus the reactor will not have any detrimental effects in case of any abnormal operations resulting in temperature increase.

5. Conclusion

Neutronics and kinetic parameters of GHARR-1's HEU reactor core after 19 years subject to addition of 9.0 mm of beryllium to the top shim tray have been observed to be within the acceptable operating margins. The parameters were in good agreement with those of the core provided in the initial SAR. The accumulation of fission products and neutron poisons in the fuel meat had some effects on various parameters despite addition of beryllium. This caused some parameters under this work to either be higher or lower compared to those provided in the initial SAR. However, neutronic and kinetic parameters were observed to be within the allowed margins and as such the reactor was safe to operate with the addition of 9.0 mm of beryllium which compensated for the reactivity loss. The results obtained under this work are fit to be used as a basis for comparing operating conditions of the LEU cores and also for future works to be carried out on the LEU core model.

Acknowledgements

The authors acknowledge the financial support given by the International Atomic Energy Agency (IAEA) and the Zambian Government through the National Institute for Scientific and Industrial Research (NISIR) to carry out this work. The Ghana Atomic Energy Commission (GHAEC) is acknowledged for authorizing access to the Ghana Research Reactor-1 and provision of information that was important for executing this work. The authors also recognise and appreciate the contribution made by members of staff under the Nuclear Engineering department of the Graduate School of Nuclear and Allied Sciences (SNAS) who contributed to the success of carrying out this work.

Table 4. Reactivity coefficients.

Parameter	Temperature Range (˚C)	Irradiated Core (mk/˚C)	Clean Core (mk/˚C)
Fuel Temperature Reactivity Coefficient	20 - 40	−0.00347	
	50 - 100	−0.00294	
	200 - 600	−0.00266	-
Average (mk/˚C)		−0.00303	-
Moderator Void	20 - 40	−0.08644	
Reactivity Coefficient	50 - 100	−0.19194	
Average (mk/˚C)		−0.13871	-
Moderator Temperature (only) Reactivity Coefficient	20 - 40	0.007848	
	50 - 100	0.003924	
Average (mk/˚C)		0.005886	
Combined Moderator	20 - 40	−0.08921	
Reactivity Coefficient	50 - 100	−0.15456	
Average (mk/˚C)		−0.12188	−0.13 (SAR)

Conflicts of Interest

The authors declare no conflicts of interest regarding the publication of this paper.

References

[1] Physics Section International Atomic Energy Agency (1980) Research Reactor Core Conversion from the Use of Highly Enriched Uranium to the Use of Low Enriched Uranium Fuels. IAEA-TECDOC-233, Vienna.

[2] Mweetwa, B.M., Ampomah-Amoako, E. and Akaho, E.H.K. (2015) Evaluation of Safety Parameters for Ghana Research Reactor-1 after Nineteen (19) Years of Operation Using REBUS/ANL, MCNP5, PARET/ANL and PLTEMP/ANL Simulation Codes. University of Ghana, Accra.

[3] Odoi, H.C., Akaho, E.H.K., Nyarko, B.J.B., Abrefah, R.G., Ampomah-Amoako, E., Sogbadji, R.B.M. and Birikorang, S.A. (2012) Conversion of International MNSR—Reference Case of Ghana MNSR. RERTR 2012, 34*th International Meeting on Reduced Enrichment for Research and Test Reactors*, Warsaw, 14-17 October 2012, S12-P2.

[4] Akaho, E.H.K., Anim-Sampong, S., Dodoo-Amoo, D.N.A., Maakuu, B.T., Emi Reynolds, G., Osae, E.K., Boadu, H.O. and Bamford, S.A. (2003) Ghana Research Reactor-1 Final Safety Analysis Report. Ghana Atomic Energy Technical Report. GAEC-NNRI, RT-90, GEAC, Accra.

[5] Adoo, N.A., Nyarko, B.J.B., Akaho, E.H.K., Alhassan, E., Agbodemegbe, V.Y., Ban-

sah, C.Y. and Della, R. (2011) Determination of Thermal Hydraulic Data of GHARR-1 under Reactivity Insertion Transients Using the PARET/ANL Code. *Nuclear Engineering and Design*, **241**, 5203-5210.

[6] Cardoni, J.N. (2011) Nuclear Reactor Multi-Physics Simulations with Coupled MCNP5 and STAR-CCM+. *International Conference on Mathematics and Computational Methods Applied to Nuclear Science and Engineering* (*M&C* 2011), Rio de Janeiro, May 8-12, 2011, 3.

[7] http://www.nuclear-power.net/nuclear-power/reactor-physics/reactor-dynamics/reactor-kinetics/

[8] Khan, M.J.H. and Islam, S.M.A. (2013) Analysis of Kinetic Parameters of 3 MW TRIGA MARK-II Research Reactor Using SRAC 2006 Code System. *Annals of Nuclear Energy*, **60**, 181-186.

[9] Farshad, F., Khalafi H. and Mirvakili, S.M. (2011) A Literature Survey of Neutronics and Thermal-Hydraulics Codes for Investigating Reactor Core Parameters; Artificial Neural Networks as the VVER-1000 Core Predictor. Nuclear Power Pavel Tsvetkov, IntechOpen. https://doi.org/10.5772/16521

[10] Broeders, C.H.M. (2000) A Comparison of Some Neutronics Characteristics of Critical Reactors and Accelerator Driven Subcritical Systems. Forschungszentrum Karlsruhe, Karlsruhe, Germany.

[11] http://www.nuclear-power.net/nuclear-power/fission/prompt-neutrons/prompt-generation-time-mean-generation-time/

[12] Bretscher, M.M. (1997) Perturbation-Independent Methods for Calculating Research Reactor Kinetic Parameters. ANL/RERTR/TM-30, Argonne National Laboratory.

[13] Suvdantsetseg, E. and Wallenius, J. (2014) An Assessment of Prompt Neutron Reproduction Time in a Reflector Dominated Fast Critical System: ELECTRA. *Annals of Nuclear Energy*, **71**, 159-165. https://doi.org/10.1016/j.anucene.2014.04.001

[14] Diagnostics Applications Group (X-5) (2000) MCNP—A General Monte Carlo N—Particle Transport Code. Version 4C, LA-13709-M Manual, Applied Physics Division (X Division), Los Alamos National Laboratory, Radiation Safety Information Computational Center (RSICC), Oak Ridge, TN, 37831-6362.

[15] X-5 Monte Carlo Team (2008) MCNP—A General Monte Carlo N—Particle Transport Code. Version 5.

[16] Daniel, J.S. (2013) A Safety Analysis of an Accidental Reactivity Excursion in the University of Florida Training Reactor (UFTR). University of Florida, 202 Nuclear Science Center, Gainesville, FL, 32611-8300.

[17] Michalek, S., Hascik, J. and Farkas, G. (2008) MCNP5 Delayed Neutron Fraction Calculation for Training Reactor VR-1. *Journal of Electrical Engineering*, **59**, 221-224.

[18] Hanson, A.L. and Diamond, D.J. (2012) Calculation of Kinetics Parameters for the NBSR. Nuclear Science and Technology Department, Brookhaven National Laboratory Upton, NY. https://doi.org/10.2172/1043393

World Journal of Nuclear Science and Technology, 2018, 8, 176-189
http://www.scirp.org/journal/wjnst
ISSN Online: 2161-6809
ISSN Print: 2161-6795

Assessment of Exposure Due to Technologically Enhanced Natural Radioactivity in Various Samples of Moroccan Building Materials

Bouchaib Kassi[1], Aziz Boukhair[1,2*], Khadija Azkour[3], Mohamed Fahad[1], Mohammed Benjelloun[1], Abdel-Mjid Nourreddine[4]

[1]Laboratory of Physics and Nuclear Techniques, Atomic and Molecular, Chouaib Doukkali University, El Jadida, Morocco
[2]Regional Center of the Trades of Education and Training, El Jadida, Morocco
[3]Ministère de l'Intérieur, El Jadida, Morocco
[4]Groupe RaMsEs, Institut Pluridisciplinaire Hubert Curien (IPHC), Université de Strasbourg, Strasbourg, France
Email: *mouad.boukhair@gmail.com

How to cite this paper: Kassi, B., Boukhair, A., Azkour, K., Fahad, M., Benjelloun, M. and Nourreddine, A.-M. (2018) Assessment of Exposure Due to Technologically Enhanced Natural Radioactivity in Various Samples of Moroccan Building Materials. *World Journal of Nuclear Science and Technology*, **8**, 176-189.
https://doi.org/10.4236/wjnst.2018.84015

Received: September 10, 2018
Accepted: October 19, 2018
Published: October 22, 2018

Abstract

The aim of our present work is to measure the specific activities of the radionuclides ^{226}Ra, ^{232}Th, ^{40}K and the exhalation rates in terms of area and mass of ^{222}Rn in some samples of building materials commonly used in Morocco in order to evaluate the radiological risk caused by natural radioactivity. To this end, the analyses were carried out, using two nuclear techniques, namely high resolution gamma spectrometry and alpha dosimetry based on the use of LR115, on 50 samples collected from large commercial suppliers in Morocco. The results of these analyses show that the average specific activities of ^{226}Ra, ^{232}Th and ^{40}K in these materials vary from 9 to 52 Bq/kg, 3 to 63 Bq/kg and 68 to 705 Bq/kg respectively. These activities remain within the permissible limits of 35 Bq/kg, 30 Bq/kg and 370 Bq/kg respectively, with the exception of a few samples of red brick, gray cement, ceramic and granite. The activity of the radium equivalent (Ra_{eq}), the internal (H_{in}) and external (H_{ex}) hazard indices, the absorbed dose rate ($\dot{D}$), the total annual effective dose ($\dot{E}_{tot}$), the excess lifetime cancer risk (ELCR) as well as volumic activities, exhalation rates in terms of area (E_S) and mass (E_M) are calculated for the samples analyzed in this work in order to assess the radiological risks resulting from the use of these materials in various construction activities. It seems that the values of these indices vary from 19 to 196 Bq/kg, 0.08 to 0.67, 0.05 to 0.53, 9 to 91 nGy/h, 0.05 to 0.56 mSv/y, 0.19×10^{-3} to 1.96×10^{-3}, 72 to 350 Bq/m^3, 56 to 273 mBq·m^{-2}·h^{-1} and 3 to 15 mBq·kg^{-1}·h^{-1} respectively. The lowest values are identified for gypsum, while the highest are attributed to granite. All of the obtained results of these indices respect the permissible limits except for

the Ra_{eq} in some granite samples, the ELCR index in all samples except gypsum and the radon volumic activity in some gray cement samples, ceramic and granite. As a result, the different types of building materials analyzed in our work do not present a health risk to the public and can be used in various construction activities, with the exception of a few samples of red brick, gray cement, ceramic and granite. The choice of the use of red brick, gray cement and ceramic should be monitored and adapted according to the criteria of the limitation of the doses whereas the use of the granite must be moderate in order to limit over time the health risk which increases with the duration of exposure of humans to these building materials.

Keywords

Building Materials, Natural Radioactivity, Radionuclide, Radon Exhalation Rate, Radium Equivalent, Annual Effective Dose

1. Introduction

Since 1970, indoor air quality has become a major preoccupation for public health, due in part to the time we spend indoors (on average 87%) [1] and the high diversity of the airborne contaminants found therein, biological, chemical and physical [2]. Building materials represent a continuous source of natural radiation because it is produced from rocks and soils that contain radioactivity at varying levels depending on their origins [3] [4]. Radioactive exposure to building materials can be divided into internal and external exposure. This latter is due to gamma radiation from the different radionuclides of the three radioactive decay chains (^{238}U, ^{235}U, ^{232}Th) and ^{40}K. Internal exposure is due to the inhalation of radon and its progeny. ^{222}Rn is now considered the main source of human exposure to natural radiation [5]. It is a naturally occurring radioactive gas from the disintegration of ^{226}Ra, itself part of the ^{238}U disintegration chain. When disintegrating, radon emits alpha particles and generates solid progeny, which are also radioactive (polonium, bismuth, lead, etc.). These descendants continue to disintegrate and emit radiation, in particular of the α and β type. Once inhaled, it dissipates their energies into the surrounding lung tissue, thereby damaging the lung cells, and altering their atomic structure. In 1987, the International Agency for Research on Cancer (IARC) of the World Health Organization (WHO) recognized radon as a pulmonary carcinogen for humans [5].

In Morocco, the building materials industry is currently experiencing significant growth. A growing demand means the creation or expansion of several production units (cement works, brickworks, etc.). In recent years, the building industry uses a raw material, large quantities of waste with a technologically enhanced natural radioactivity (coal ash, phosphogypses, etc.) [6] [7] [8]. The use of these materials in building materials has economic advantages but may affect the doses received by humans inside buildings as has been demonstrated in var-

ious studies [9] [10] [11]. Hence, the knowledge of the natural radioactivity in buildings materials from the three radioactive decay chains (^{238}U, ^{235}U, ^{232}Th) and ^{40}K, is necessary and important for the assessment of the radiological impact on the public and the environment. To evaluate the radiological impact of these materials on the population and the environment, and through these specific activities, we calculated several radiological risk indices, namely radium equivalent (Ra_{eq}), internal (H_{in}) and external (H_{ex}) hazard indices, total annual effective dose ($\dot{E}_{tot}$) as well as the excess lifetime cancer risk (ELCR).

2. Materials and Methods

2.1. Sample Preparation

The building materials samples to be analyzed are collected from large and important commercial suppliers in Morocco. As regards sand, samples are taken from seven different quarries in the Doukkala region. Before any analysis and to obtain homogeneous samples, these building materials are dried in an oven at 40˚C for 24 hours and then ground and sieved through a 100 μm mesh screen. The screened samples are packaged in radon-tight containers for at least 4 weeks to establish the secular equilibrium corresponding to seven half-lives of ^{222}Rn.

2.2. Spectroscopic Analysis

The measurement of the natural radioactivity in the prepared samples is carried out by gamma ray spectrometer using the Broad Energy Germanium detector (BEGe) at Pluridisciplinary Institute Hubert Curien in Strasbourg, France. It is a planar type Hyper-Pure Germanium HPGe detector associated with a set of electronic modules for shaping the pulses, amplifying and storing the pulses delivered during the passage of the gamma rays through the detector. Its energy measurement range is 30 to 3000 keV with a resolution of 0.633 keV to 122 keV and from 1.934 keV to 1332 keV [12].

As regards the energy and efficiency calibration of the BEGe detector, a multi-energy certified standard is analyzed under the same conditions and geometry as the samples studied. This standard contains several γ-emitting radionuclides such as ^{241}Am (60 keV), ^{109}Cd (88 keV), ^{57}Co (122, 136 keV), ^{139}Ce (165 keV), ^{51}Cr (320 keV), ^{113}Sn (391 keV), ^{85}Sr (514 keV), ^{137}Cs (661 keV), ^{88}Y (898, 1836 keV) and^{60}Co (1173, 1332 keV). Samples of building materials are packaged in SG50 geometry and counted for 172.800 seconds. The treatment of the amplitude spectra is carried out using automatic analysis software Genie 2000 [12] allowing to give directly the mass activity of each radioelement present in the sample.

The volumetric activities and the exhalation rate in terms of area and mass of the radon in the prepared samples are carried out using the alpha dosimetry. For this purpose, several pieces of 2 × 2 cm^2 of Solid State Nuclear Track Detector (SSNTD) LR115 type 2 non strippable, Kodak brand 12 μm thick, are exposed in sealed cylindrical "cans" of 5.5 cm diameter and 9.5 cm height by 50 g of each

sample of building materials. After two months of irradiation, the LR115 are chemically treated in a 2.5 N sodium hydroxide solution during 100 min at a temperature of 60˚C. The developed films are read using an optical microscope. The density of traces per unit area and per unit time in LR115 and the volume activity of radon A_V^{Rn} are determined according to [13].

3. Results and Discussions

3.1. Specific Activities

The specific activities of the radionuclides ^{226}Ra, ^{232}Th and ^{40}K are calculated by gamma spectrometry, after establishment of the secular equilibrium, in the various samples of building materials using the following ratios of energies:

- ^{214}Pb (295 keV and 352 keV) and ^{214}Bi (609 keV, 1120 keV and 1764 keV) for ^{226}Ra;
- ^{228}Ac (911 keV and 969 keV) and ^{212}Pb (239 keV) for ^{232}Th;
- ^{40}K (1461 keV) from the emission intensity line 10.55%.

Figure 1 shows the minimum, the maximum and the average specific activities of ^{226}Ra, ^{232}Th and ^{40}K radionuclides measured in the different types of

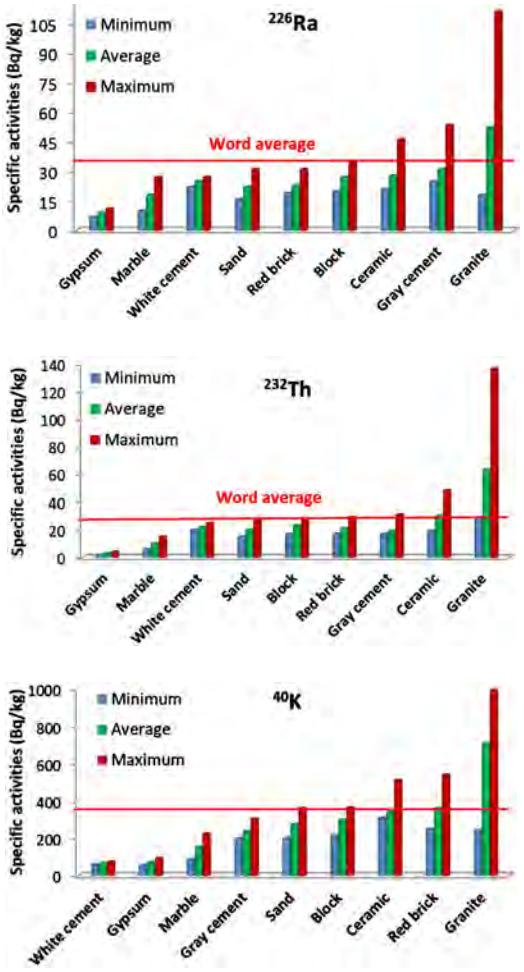

Figure 1. Specific activities of different radionuclides in Moroccan building materials.

building materials. It can be seen that the contribution of the activity of the ^{40}K is much greater than that contributed by the ^{238}U and the ^{232}Th. It should also be noted that the activity of ^{232}Th in each sample is less than that of ^{226}Ra except for the red brick, ceramic and granite samples.

From these values, it results that the low average specific activities are recorded in the gypsum for the radionuclides ^{226}Ra and ^{232}Th, and in the white cement for the ^{40}K with average activities of the order of 9 Bq/kg, 3 Bq/kg and 68 Bq/kg respectively. The highest average specific activities for the ^{226}Ra, ^{232}Th and ^{40}K radionuclides are recorded in the granite and are respectively of the order of 52 Bq/kg, 63 Bq/kg and 705 Bq/kg. All the specific activities of the measured ^{226}Ra, ^{232}Th and ^{40}K are within the permissible limits of 35 Bq/kg, 30 Bq/kg and 370 Bq/kg [4], respectively, with the exception of a few samples of red brick, gray cement, ceramic and granite. Therefore, the choice of materials for building constructions should be monitored and adapted according to the criteria of the limitation of doses.

In **Table 1**, and for comparison with our results, the specific activities of natural radionuclides are grouped together in samples of building materials in Morocco and some other countries. Overall, the specific activities obtained in this study are comparable to those found in other countries, with the exception of a few activities that are remarkably higher than ours.

3.2. Radium Equivalent

Due to the non-uniform distribution of natural radionuclides in building material samples, the radiological index radium equivalent Ra_{eq} is generally represented as the sum of the specific activities of ^{226}Ra, ^{232}Th and ^{40}K based on the assumption that 10 Bq/Kg of ^{226}Ra, 7 Bq/kg of ^{232}Th and 130 Bq/kg of ^{40}K would produce the same dose rate of gamma radiation. This is the most widely used index for radiological risk assessment. It is calculated using the following equation [5] [28]:

$$Ra_{eq} = A_{226\mathrm{Ra}} + 1.43A_{232\mathrm{Th}} + 0.077A_{40\mathrm{K}} \quad (1)$$

where $A_{226\mathrm{Ra}}$, $A_{232\mathrm{Th}}$ and $A_{40\mathrm{K}}$ are the specific activities in (Bq/kg) of ^{226}Ra, ^{232}Th and ^{40}K in the samples analyzed.

In **Table 2**, the mean values of the radium equivalent Ra_{eq} varying from 19 to 196 Bq/kg, which are still below the permissible limit of 370 Bq/kg [5], are grouped together for the samples analyzed. We note that the lowest value is found in the gypsum, while the highest is in the granite.

From these results, we can consider that these building materials do not present a significant radiological hazard to the population and can be used in various construction activities. However, it should be noted that the Ra_{eq} values vary considerably in the same type of building materials and may in some cases exceed the permissible limit. This is the case of granite where the maximum value of the equivalent radium Ra_{eq} is of the order of 382 Bq/kg. The use of the latter in construction activities must be moderate.

Table 1. Comparison between the specific activities of building materials in a few countries.

Samples	Country	Specific activities (Bq/kg)			References
		^{226}Ra	^{232}Th	^{40}K	
Gray Cement	European Union	45	31	216	[14]
	China	21.7 ± 1.92	22 ± 0.89	181 ± 3.75	[15]
	Turkey	39.9 ± 18.0	26.4 ± 9.8	316.5 ± 88.1	[16]
	South Korea	34.5 ± 1.7	19.4 ± 1.5	241 ± 6.7	[17]
	Morocco	31 ± 5	19 ± 3	238 ± 29	Present Work
White Cement	Egypt	17.45 ± 2.33	8.44 ± 1.49	4.09 ± 4.72	[18]
	Turkey	32.8 ± 5.1	16.3 ± 7.6	99.2 ± 31.8	[16]
	Qatar	18.9 ± 0.5	4.9 ± 0.5	62.9 ± 22.6	[19]
	Serbia	18 ± 3	12 ± 5	55 ± 37	[20]
	Iraq	49.577 ± 0.865	16.74 ± 2.28	32.6 ± 4.31	[21]
	Morocco	25 ± 4	22 ± 3	68 ± 8	Present Work
Gypsum	Saudi Arabia	33.28 ± 4.7	47.2 ± 2.8	88 ± 4.4	[22]
	Italy	6 ± 5	2 ± 2	32 ± 43	[23]
	Iran	8.1 ± 0.1	2.2 ± 0.1	116 ± 11	[24]
	Morocco	9 ± 1	3 ± 1	73 ± 9	Present Work
Red brick	Iran	37.0 ± 1.5	12.2 ± 0.7	851 ± 15	[24]
	Albania	33.4 ± 6.4	42.2 ± 7.6	644.1 ± 64.2	[25]
	Egypt	23.06 ± 2.60	23.11 ± 2.99	447.84 ± 10.16	[18]
	Morocco	23 ± 4	21 ± 3	360 ± 41	Present Work
Block	Egypt	288.5 ± 17.49	77.77 ± 15.61	909.5 ± 59.73	[18]
	Iran	20.7 ± 1.1	3.0 ± 0.4	436 ± 14	[24]
	Morocco	27 ± 3	23 ± 3	300 ± 37	Present Work
Ceramic	Egypt	51.12 ± 2.74	40.52 ± 2.54	682.6 ± 10.13	[18]
	Turkey	33.1 ± 2.5	49.5 ± 3.3	459.1 ± 51.3	[26]
	Syria	65.878 ± 1.0	28.16 ± 3.0	401 ± 14.67	[21]
	Morocco	28 ± 5	30 ± 5	340 ± 42	Present Work
Marble	Saudi Arabia	12.7 ± 3.4	13.2 ± 1.4	64 ± 3	[22]
	Algeria	23 ± 2	18 ± 2	310 ± 3	[27]
	Morocco	18 ± 2	10 ± 1	154 ± 19	Present Work
Granite	Saudi Arabia	23 ± 1.4	30.0 ± 0.4	340 ± 6.7	[22]
	Turkey	67.5 ± 47.6	77.4 ± 53.0	915.3 ± 361.2	[16]
	Morocco	52 ± 6	63 ± 8	705 ± 84	Present Work
Sand	Turkey	38.8 ± 10.0	29.5 ± 11.3	471.4 ± 101.2	[26]
	Qatar	13.2 ± 0.3	3.34 ± 0.05	225.5 ± 6.1	[19]
	Pakistan	21.5 ± 0.5	31.9 ± 0.5	519.6 ± 6.0	[28]
	Morocco	22 ± 3	20 ± 3	274 ± 47	Present Work

Table 2. Average values of radium equivalent, hazard indices, absorbed dose rate, annual effective dose and the excess lifetime cancer risk in the samples of building materials analyzed.

Samples	Ra_{eq} (Bq/kg)	H_{in}	H_{ex}	$\dot{D}$ (nGy/h)	$\dot{E}_{in}$ (mSv/y)	$\dot{E}_{ex}$ (mSv/y)	$\dot{E}_{tot}$ (mSv/y)	ELCR ($\times 10^{-3}$)
Graycement	77 ± 7	0.29 ± 0.05	0.21 ± 0.04	36 ± 2	0.18 ± 0.04	0.04 ± 0.01	0.18 ± 0.04	0.77 ± 0.06
Gypsum	19 ± 2	0.08 ± 0.02	0.05 ± 0.02	9 ± 1	0.04 ± 0.01	0.01 ± 0.01	0.04 ± 0.01	0.19 ± 0.01
Whitecement	62 ± 4	0.23 ± 0.04	0.17 ± 0.03	28 ± 1	0.14 ± 0.03	0.03 ± 0.01	0.14 ± 0.03	0.60 ± 0.05
Red brick	82 ± 12	0.28 ± 0.04	0.22 ± 0.04	39 ± 4	0.19 ± 0.04	0.05 ± 0.01	0.19 ± 0.04	0.83 ± 0.07
Block	82 ± 11	0.30 ± 0.05	0.22 ± 0.04	39 ± 3	0.19 ± 0.04	0.05 ± 0.01	0.19 ± 0.04	0.83 ± 0.07
Ceramic	97 ± 14	0.34 ± 0.05	0.26 ± 0.05	45 ± 5	0.22 ± 0.05	0.06 ± 0.02	0.22 ± 0.05	0.97 ± 0.09
Marble	45 ± 4	0.17 ± 0.03	0.12 ± 0.02	21 ± 1	0.10 ± 0.03	0.03 ± 0.01	0.10 ± 0.03	0.45 ± 0.04
Granite	196 ± 17	0.67 ± 0.06	0.53 ± 0.05	91 ± 7	0.45 ± 0.08	0.11 ± 0.03	0.45 ± 0.08	1.96 ± 0.10
Sand	72 ± 8	0.26 ± 0.04	0.20 ± 0.04	34 ± 3	0.17 ± 0.04	0.04 ± 0.01	0.17 ± 0.04	0.73 ± 0.07

3.3. Internal and External Hazard Indices

The calculation of the total activity of radionuclides in building materials alone does not make it possible to assess the radiological risks of gamma radiation. Other risk indices are also taken into account and are defined by a model taking into account the maximum activity of Ra_{eq} (370 Bq/kg). The external hazard index H_{ex} is defined by the following equation [5] [28]:

$$H_{ex} = \frac{A_{226\mathrm{Ra}}}{370} + \frac{A_{232\mathrm{Th}}}{259} + \frac{A_{40\mathrm{K}}}{4810} \tag{2}$$

In addition to this external hazard, the respiratory organs are threatened because of the decay of ^{226}Ra into ^{222}Rn and its descendants. To account for this threat, the maximum permissible activity for ^{226}Ra is therefore reduced by half (185 Bq/kg). This internal hazard H_{in} is quantified by the following relation [5] [28]:

$$H_{in} = \frac{A_{226\mathrm{Ra}}}{185} + \frac{A_{232\mathrm{Th}}}{259} + \frac{A_{40\mathrm{K}}}{4810} \tag{3}$$

Table 2 gives the internal and external hazard indices of the samples of the building materials studied. The values of the internal hazard index according to the materials vary between 0.08 and 0.67 while for the external hazard index they are between 0.05 and 0.53. The values are maximum for granite and minimum for gypsum. None of these values exceeds the unit, the maximum value of the internal (H_{in}) and external (H_{ex}) hazard indices allowed.

3.4. Absorbed Dose Rate and Annual Effective Dose

The absorbed dose rate $\dot{D}$ (nGy/h) due to the specific activity of natural radionuclides from building materials in air at 1 m height is defined by the following equation [5]:

$$\dot{D}(\mathrm{nGy/h}) = 0.462A_{226\mathrm{Ra}} + 0.604A_{232\mathrm{Th}} + 0.0417A_{40\mathrm{K}} \tag{4}$$

Table 2 summarizes the results of the absorbed dose rates in air for the analyzed building materials. We note that the highest value is attributed to granite (91 nGy/h) while the lowest value is gypsum (9 nGy/h). These values of absorbed dose rates are below the permissible limit (55 nGy/h) [5] with the exception of the granite sample.

To estimate the annual effective dose received by the population, we take into account the coefficient of conversion of dose rate absorbed in air in effective dose (0.7 Sv/Gy) and external occupancy factor (0.2) [5]. The annual effective doses are determined as follows [5]:

$$\dot{E}_{ex}\left(\mathrm{mSv/y}\right)=\dot{D}\left(\mathrm{nGy/h}\right)\times 8760\left(\mathrm{h}\right)\times 0.2\times 0.7\left(\mathrm{Sv/Gy}\right)10^{-6} \quad (5)$$

$$\dot{E}_{in}\left(\mathrm{mSv/y}\right)=\dot{D}\left(\mathrm{nGy/h}\right)\times 8760\left(\mathrm{h}\right)\times 0.8\times 0.7\left(\mathrm{Sv/Gy}\right)10^{-6} \quad (6)$$

The results of the annual external ($\dot{E}_{ex}$), internal ($\dot{E}_{in}$) and total ($\dot{E}_{tot}$) effective doses for the samples of building materials studied are given in Table 2. It is found that the total value for each sample is less than the annual effective dose limit set at 1 mSv/y [5]. Therefore, we consider that these building materials do not present a radiological risk to the population and can be used in the construction of buildings.

3.5. Excess Lifetime Cancer Risk

The Excess Lifetime Cancer Risk (ELCR) treats the probability of developing cancer during the life of a human being at a certain level of exposure. The ELCR is calculated using the following equation [29]:

$$\mathrm{ELCR}=\dot{E}_{tot}\times \mathrm{DL}\times \mathrm{RF} \quad (7)$$

Or:

$\dot{E}_{tot}$ is the total annual effective dose (μSv/year);

DL (Duration of Life) is the average life span of a human being (70 years);

RF is the Risk Factor fatal by cancer (Sv^{-1}). For stochastic effects, the International Commission on Radiological Protection (ICRP) estimates the value of this factor to be 0.05 for the public [30].

In Table 2, ELCR values range from 0.19×10^{-3} to 1.96×10^{-3} where the lowest value is found in the gypsum, while the highest is in the granite. The ELCR value at the granite sample far exceeds the permissible limit of 0.29×10^{-3} [29]. As a result, the risk of cancer increases with increasing exposure to these materials.

3.6. Volume Activities and Radon Exhalation Rates

After calculating the density of traces per unit area and per unit time in the LR115, the volume activities of the radon A_V^{Rn} are calculated using the detection efficiency equal to 0.0258 $(\mathrm{traces\cdot cm^{-2}\cdot j^{-1}})/(\mathrm{Bq\cdot m^{-3}})$ [31]. The exhalation rate in terms of area (E_S in $\mathrm{Bq\cdot m^{-2}\cdot h^{-1}}$) and mass ($E_M$ in $\mathrm{Bq\cdot kg^{-1}\cdot h^{-1}}$) of ^{222}Rn are determined by the following equation [32] [33]:

$$E_S = \frac{A_V^{Rn} V \lambda_{Rn}}{S_e \left[t + \left(\frac{1}{\lambda_{Rn}} \right) \left(e^{-\lambda_{Rn} t} - 1 \right) \right]} \quad (8)$$

$$E_M = \frac{A_V^{Rn} V \lambda_{Rn}}{M \left[t + \left(\frac{1}{\lambda_{Rn}} \right) \left(e^{-\lambda_{Rn} t} - 1 \right) \right]} \quad (9)$$

With A_V^{Rn} is the volume activity of radon ($Bq \cdot m^{-3} \cdot h$); V is the volume of the enclosure (m^3); λ_{Rn} is the ^{222}Rn decay constant (h^{-1}); S_e is the area of the sample (m^2); M is the mass of the sample in kg and t is the exposure time (h).

We present in **Table 3** the average values of the volumetric activity and exhalation rate in terms of area and mass of radon measured in the samples of the building materials analyzed. These values vary respectively from (72 to 350 Bq/m^3), (56 to 273 $mBq \cdot m^{-2} \cdot h^{-1}$) and (3 to 15 $mBq \cdot kg^{-1} \cdot h^{-1}$) where the lowest values are identified in the gypsum, while the highest values are in the granite. All volumic activity values for radon are in the range of 100 to 300 Bq/m^3 recommended by ICRP [34] with the exception of some samples of gray cement (191 to 366 Bq/m^3), ceramic (159 to 322 Bq/m^3) and granite (132 to 610 Bq/m^3).

In **Table 4**, for comparison with our results, the volumetric activities and exhalation rates in terms of area and mass of radon in building materials samples in Morocco and some other countries. Overall, the obtained results in this study are comparable to those found in other countries, with the exception of a few values that are remarkably higher than ours.

A positive correlation is found between the specific activities of ^{226}Ra on the one hand, it is determined by high resolution gamma spectrometry and the exhalation rates of ^{222}Rn calculated with the alpha dosimetry based on the use of LR115 on the other hand. This correlation is illustrated in **Figure 2** with a correlation coefficient in the order of 0.96.

Table 3. Volume activity and exhalation rate of radon in different samples of Moroccan building materials.

Samples		A_V^{Rn} (Bq/m^3)		E_S ($mBq \cdot m^{-2} \cdot h^{-1}$)		E_M ($mBq \cdot kg^{-1} \cdot h^{-1}$)	
Type	Nr.	Range	Average	Range	Average	Range	Average
Gray cement	7	191 - 366	248 ± 26	149 - 286	194 ± 21	8 - 15	10 ± 2
Gypsum	5	54 - 92	72 ± 7	42 - 72	56 ± 4	2 - 4	3 ± 1
White cement	5	184 - 198	191 ± 19	144 - 155	149 ± 15	7 - 8	7 ± 1
Red brick	5	130 - 192	159 ± 16	101 - 150	124 ± 13	5 - 8	7 ± 1
Block	5	140 - 211	176 ± 19	109 - 165	137 ± 19	6 - 9	7 ± 1
Ceramic	6	159 - 322	226 ± 22	124 - 251	176 ± 18	7 - 13	10 ± 2
Marble	5	69 - 220	151 ± 16	54 - 172	118 ± 12	3 - 9	6 ± 1
Granite	5	132 - 610	350 ± 34	103 - 476	273 ± 26	5 - 25	15 ± 3
Sand	7	140 - 275	190 ± 20	109 - 215	148 ± 16	6 - 11	8 ± 1

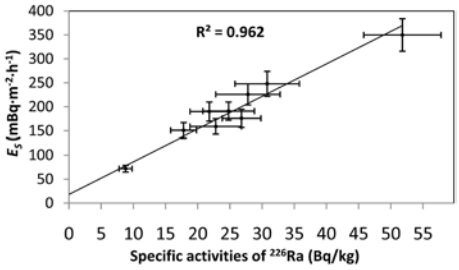

Figure 2. Correlation between the specific activities of ^{226}Ra and the exhalation rate of ^{222}Rnin building materials samples.

Table 4. Comparison between the Radon volume activities and the exhalation rates of radon in building materials in a few countries.

Samples	Country	A_V^{Rn} (Bq/m^3)	E_S (mBq·m^{-2}·h^{-1})	E_M (mBq·Kg^{-1}·h^{-1})	References
Gray cement	India	307	244	11.2	[35]
	Jordan	177	90	6	[36]
	Morocco	248	194	10	Present Work
Cement White	Palestine	102	63	6.4	[37]
	India	365	288	13.3	[35]
	Morocco	191	149	7	Present Work
Gypsum	Saudi Arabia	157.5	145.7	4.6	[38]
	Algeria	42	36	-	[39]
	Morocco	72	56	3	Present Work
Brick red	Algeria	166	101	-	[39]
	Morocco	159	124	7	Present Work
Block	India	235	241	-	[40]
	Jordan	160	82	6	[36]
	Morocco	176	137	7	Present Work
Ceramic	Algeria	75	65	-	[39]
	Palestine	132	75	3.2	[37]
	Morocco	226	176	10	Present Work
Marble	Algeria	56	48	-	[39]
	Libya	264.6	212.7	9.8	[41]
	Saudi Arabia	76.4	72.3	-	[38]
	Morocco	151	118	6	Present Work
Granite	Palestine	246	146	7.2	[37]
	Morocco	350	273	15	Present Work
Sand	Palestine	84	48	2.4	[37]
	Jordan	267	149	14	[36]
	Morocco	190	148	8	Present Work

4. Conclusion

In this present work, we used gamma spectrometry to determine natural radioactivity in 50 samples of building materials commonly used in Morocco. The specific activities of the ^{226}Ra, ^{232}Th and ^{40}K radionuclides measured in these samples vary from 9 to 52 Bq/kg, from 3 to 63 Bq/kg and from 68 to 705 Bq/kg respectively. These activities of the studied samples are within the permissible limits with the exception of a few samples of red brick, gray cement, ceramic and granite. To evaluate the radiological impact of these building materials on the population, the environment and through these specific activities, we calculated several radiological risk indices, namely radium equivalent (Ra_{eq}), internal (H_{in}) and external (H_{ex}) hazard indices, the absorbed dose rate ($\dot{D}$), the total annual effective dose ($\dot{E}_{tot}$), the excess lifetime cancer risk (ELCR), the volume activities (A_V^{Rn}) and the exhalation rate in terms of area (E_S) and mass (E_M). It follows that the values of these indices vary from 19 to 196 Bq/kg, 0.07 to 0.67, 0.05 to 0.53, 9 to 91 nGy/h, 0.05 to 0.56 mSv/y, 0.19×10^{-3} to 1.96×10^{-3}, 72 to 305 Bq/m^3, 56 to 273 mBq·m^{-2}·h^{-1} and 3 to 15 mBq·kg^{-1}·h^{-1} respectively. The lowest values are identified for gypsum, while the highest are attributed to granite. All of the obtained results of these indices respect the permissible limits except for the Ra_{eq} in some granite samples, the ELCR index in all samples except gypsum and the radon volumic activity in some gray cement samples, ceramic and granite. Consequently, the different types of building materials analyzed in this work do not present any significant health risks to the public and can be used in various construction activities with the exception of a few samples of red brick, gray cement, ceramic and granite. The choice of the use of red brick, gray cement and ceramic should be monitored and adapted according to the criteria of the limitation of the doses whereas the use of the granite must be moderate in order to limit over time the health risk which increases with the duration of exposure of humans to these building materials.

Conflicts of Interest

The authors declare no conflicts of interest regarding the publication of this paper.

References

[1] Klepeis, N.E., Nelson, W.C., Ott, W.R., Robinson, J.P., Tsang, A.M., Switzer, P., Behar, J.V., Hern, S.C. and Engelmann, W.H. (2001) The National Human Activity Pattern Survey (NHAPS): A Resource for Assessing Exposure to Environmental Pollutants. *Journal of Exposure Analysis and Environmental Epidemiology*, **11**, 231-252. https://doi.org/10.1038/sj.jea.7500165

[2] Salthammer, T. and Bahadir, M. (2009) Occurrence, Dynamics and Reactions of Organic Pollutants in the Indoor Environment. *CLEAN—Soil Air Water*, **37**, 417-435. https://doi.org/10.1002/clen.200900015

[3] Alance, M., Gaidolfi, L., Pessina, V. and Dallara, G. (1996) Distribution of ^{226}Ra, ^{232}Th, and ^{40}K in Soils of Rio Grande do Norte (Brazil). *Journal of Environmental*

Radioactivity, **30**, 55-67. https://doi.org/10.1016/0265-931X(95)00035-9

[4] United Nations Scientific Committee on the Effects of Atomic Radiation (UNSCEAR) (2000) Sources and Effects of Ionizing Radiation. United Nations, New York.

[5] United Nations Scientific Committee on the Effects of Atomic Radiation (UNSCEAR) (2006) Sources and Effects of Ionizing Radiation. United Nations, New York.

[6] Iyer, R.S. and Scott, J.A. (2001) Power Station Fly Ash—A Review of Value-Added Utilization outside of the Construction Industry. *Resources, Conservation and Recycling*, **31**, 217-228. https://doi.org/10.1016/S0921-3449(00)00084-7

[7] Pantazopoulou, E., Zebiliadou, O., Bartzas, G., Xenidis, A., Zouboulis, A. and Komnitsas, K. (2015) Industrial Solid Waste Management in Greece: The Current Situation and Prospects for Valorization. *Journal of Solid Waste Technology and Management*, **41**, 383-394.

[8] Radiological Protection Principles Concerning the Natural Radioactivity of Building Materials. https://ec.europa.eu/energy/sites/ener/files/documents/112.pdf

[9] Saravanan, S., Jodha, A.S., Gopalani, D., Bhati, S.S. and Kumar, S. (2003) Preliminary Measurements of Natural Radioactivity at Madurai District of Tamilnadu, India. *Radiation Measurements*, **36**, 397-399. https://doi.org/10.1016/S1350-4487(03)00159-8

[10] Medhat, M.E. and Fayez-Hasssan, M. (2010) Natural Radioactivity of Egyptian Building Materials. *Arab Journal of Nuclear Sciences and Applications*, **43**, 151-160.

[11] Szabó, Z., Völgyesi, P., Nagy, H.É., Szabó, C., Kis, Z. and Csorba, O. (2013) Radioactivity of Natural and Artificial Building Materials—A Comparative Study. *Journal of Environmental Radioactivity*, **118**, 64-74. https://doi.org/10.1016/j.jenvrad.2012.11.008

[12] (2005) Genie 2000, Version 3.2. Canberra Industries, Inc., Canberra France HQ & Europe Coordination Bois Mouton, Canberra.

[13] Boukhair, A., Belahbib, L., Azkour, K., Nebdi, H., Benjelloun, M. and Nourreddine, A. (2016) Measurement of Natural Radioactivity and Radon Exhalation Rate in Coal Ash Samples from a Thermal Power Plant. *World Journal of Nuclear Science and Technology*, **6**, 153-160. https://doi.org/10.4236/wjnst.2016.63017

[14] Trevisi, R., Risica, S., D'Alessandro, M., Paradiso, D. and Nuccetelli, C. (2012) Natural Radioactivity in Building Materials in the European Union: A Database and an Estimate of Radiological Significance. *Journal of Environmental Radioactivity*, **105**, 11-20. https://doi.org/10.1016/j.jenvrad.2011.10.001

[15] Yu, K.N., Guan, Z.J., Stokes, M.J. and Young, E.C.M. (1992) The Assessment of the Natural Radiation Dose Committed to the Hong Kong People. *Journal of Environmental Radioactivity*, **17**, 31-48. https://doi.org/10.1016/0265-931X(92)90033-P

[16] Turhan, Ş., Baykan, U.N. and Şen, K. (2008) Measurement of the Natural Radioactivity in Building Materials Used in Ankara and Assessment of External Doses. *Journal of Radiological Protection*, **28**, 83-91. https://doi.org/10.1088/0952-4746/28/1/005

[17] Lee, S.C., Kim, C.K., Lee, D.M. and Kang, H.D. (2001) Natural Radionuclides Contents and Radon Exhalation Rates in Building Materials Used in South Korea. *Radiation Protection Dosimetry*, **94**, 269-274. https://doi.org/10.1093/oxfordjournals.rpd.a006499

[18] Shoeib, M.Y. and Thabayneh, K.M. (2014) Assessment of Natural Radiation Expo-

sure and Radon Exhalation Rate in Various Samples of Egyptian Building Materials. *Journal of Radiation Research and Applied Sciences*, **7**, 174-181. https://doi.org/10.1016/j.jrras.2014.01.004

[19] Al-Sulaiti, H., Alkhomashi, N., Al-Dahan, N., Al-Dosari, M., Bradley, D.A., Bukhari, S., Matthews, M., Regan, P.H. and Santawamaitre, T. (2001) Determination of the Natural Radioactivity in Qatarian Building Materials Using High-Resolution Gamma-Ray Spectrometry. *Nuclear Instruments and Methods in Physics Research A*, **652**, 915-919. https://doi.org/10.1016/j.nima.2011.01.020

[20] Manić, G., Manić, V., Nikezić, D. and Krstić, D. (2015) The Dose of Gamma Radiation from Building Materials and Soil. *NUKLEONIKA*, **60**, 951-958. https://doi.org/10.1515/nuka-2015-0148

[21] Najam, L.A., Tawfiq, N.F. and Kitah, F.H. (2013) Measurement of Natural Radioactivity in Building Materials Used in IRAQ. *Australian Journal of Basic and Applied Sciences*, **7**, 56-66.

[22] El-Taher, A. (2012) Assessment of Natural Radioactivity Levels and Radiation Hazards for Building Materials Used in Qassim Area, Saudi Arabia. *Romanian Journal of Physics*, **57**, 726-735.

[23] Rizzo, S., Brai, M., Basile, S., Bellia, S. and Hauser, S. (2001) Gamma Activity and Geochemical Features of Building Materials: Estimation of Gamma Dose Rate and Indoor Radon Levels in Sicily. *Applied Radiation and Isotopes*, **55**, 259-265. https://doi.org/10.1016/S0969-8043(00)00384-5

[24] Mehdizadeh, S., Faghihi, R. and Sina, S. (2011) Natural Radioactivity in Building Materials in Iran. *NUKLEONIKA*, **56**, 363-368.

[25] Xhixha, G., Ahmeti, A., Bezzon, G.P., Bitri, M., Broggini, C., Buso, G.P., Caciolli, A., Callegari, I., Cfarku, F., Colonna, T., Fiorentini, G., Guastaldi, E., Mantovani, F., Massa, G., Menegazzo, R., Mou, L., Prifti, D., Rossi Alvarez, C., Sadiraj Kuqi, Dh., Shyti, M., Tushe, L., Xhixha Kaçeli, M. and Zyfi, A. (2013) First Characterization of Natural Radioactivity in Building Materials Manufactured in Albania. *Radiation Protection Dosimetry*, **155**, 217-223. https://doi.org/10.1093/rpd/ncs334

[26] Solak, S., Turhan, S., Ugur, F.A., Goren, E., Gezer, F., Yegingil, Z. and Yegingil, I. (2012) Evaluation of Potential Exposure Risks of Natural Radioactivity Levels Emitted from Building Materials Used in Adana, Turkey. *Indoor and Built Environment*, **23**, 594-602. https://doi.org/10.1177/1420326X12448075

[27] Amrani, D. and Tahtat, M. (2001) Natural Radioactivity in Algerian Building Materials. *Applied Radiation and Isotopes*, **54**, 687-689. https://doi.org/10.1016/S0969-8043(00)00304-3

[28] Tufail, M., Ahmad, N., Mirza, S.M., Mirza, N.M. and Khan, H.A. (1992) Natural Radioactivity from the Building Materials Used in Islamabad and Rawalpindi, Pakistan. *The Science of the Total Environment*, **121**, 283-291. https://doi.org/10.1016/0048-9697(92)90321-I

[29] Hayambu, P., Zaman, M.B., Lubaba, N.C.H., Munsanje, S.S. and Muleya, D. (1995) Natural Radioactivity in Zambian Building Materials Collected from Lusaka. *Journal of Radioanalytical and Nuclear Chemistry*, **199**, 229-238. https://doi.org/10.1007/BF02162371

[30] International Commission on Radiological Protection (1990) Recommendations of the International Commission on Radiological Protection. *Annals of the ICRP*, **21**, 1-3.

[31] Pape, A., Adloff, J.C., Barillon, R., Haessler, A., Hoernel, A., Nourreddine, A., Oster, D. and Weidmann, D. (1998) Quantitative Alpha-Particle Detection in a Homoge-

neous Medium with LR115. *Nuclear Instruments and Methods in Physics Research Section B*: *Beam Interactions with Materials and Atoms*, **143**, 557-560. https://doi.org/10.1016/S0168-583X(98)00398-X

[32] Abu-Jarad, F., Fremlin, J.H. and Bull, R. (1980) A Study of Radon Emitted from Building Materials Using Plastic α-Track Detectors. *Physics Medicine and Biology*, **25**, 683-694. https://doi.org/10.1088/0031-9155/25/4/007

[33] Khan, A.J., Prasad, R. and Tyagi, R.K. (1992) Measurement of Radon Exhalation Rate from Some Buildings Materials. *International Journal of Radiation Applications and Instrumentation*. *Part D*. *Nuclear Tracks and Radiation Measurements*, **20**, 609-610. https://doi.org/10.1016/1359-0189(92)90013-L

[34] International Commission on Radiological Protection (ICRP) (2014) Radiological Protection against Radon Exposure. *Annals of the ICRP*, **43**, 3.

[35] Nain, M., Chauhan, R.P. and Chakarvarti, S.K. (2006) Alpha Radioactivity in Indian Cement Samples. *Iranian Journal of Radiation Research*, **3**, 171-176.

[36] Ismail, A.M., Abumurad, K.M., Kullab, M.K. and Al-Bataina, B.A. (1994) Measurement of Rn-222 Concentrations in Building Materials Used in Jordan. *Mutah Journal for Research and Studies*, **28**, 1119-1127.

[37] Dabayneh, K.M. (2008) ^{222}Rn Concentration Level Measurements and Exhalation Rates in Different Types of Building Materials Used in Palestinian Buildings. *Isotope and Radiation Research*, **40**, 278-289.

[38] Amin, R.M. (2015) A Study of Radon Emitted from Building Materials Using Solid State Nuclear Track Detectors. *Journal of Radiation Research and Applied Sciences*, **8**, 516-522. https://doi.org/10.1016/j.jrras.2015.06.001

[39] Amrani, D. and Cherouati, D.E. (1999) Radon Exhalation Rate in Building Materials Using Plastic Track Detectors. *Journal of Radioanalytical and Nuclear Chemistry*, **242**, 269-271. https://doi.org/10.1007/BF02345552

[40] Pereiraa, C.E., Vaidyana, V.K., Jojoa, P.J. and Ramachandran, T.V. (2008) Measurement of Radon Exhalation Rate from Building Materials Used in the Southwest Coastal Region of India. *Indoor and Built Environment*, **17**, 472-475. https://doi.org/10.1177/1420326X08095830

[41] Saad, A.F., Hend, H., Al-Awami and Hussein, N.A. (2014) Radon Exhalation from Building Materials Used in Libya. *Radiation Physics and Chemistry*, **101**, 15-19. https://doi.org/10.1016/j.radphyschem.2014.03.030

World Journal of Nuclear Science and Technology, 2018, 8, 190-196
http://www.scirp.org/journal/wjnst
ISSN Online: 2161-6809
ISSN Print: 2161-6795

A Way to Realize Controlled Nuclear Fusion by γ-Laser or γ-Ray

Shihao Chen[1], Ziwei Chen[2]

[1]Institute of Theoretical Physics, Northeast Normal University, Changchun, China
[2]Key Laboratory of Microwave and Electromagnetic Radiation, Institute of Electronics, Chinese Academy of Science, Beijing, China

Email: shchen@nenu.edu.cn

How to cite this paper: Chen, S.H. and Chen, Z.W. (2018) A Way to Realize Controlled Nuclear Fusion by γ-Laser or γ-Ray. *World Journal of Nuclear Science and Technology*, **8**, 190-196.
https://doi.org/10.4236/wjnst.2018.84016

Received: September 3, 2018
Accepted: October 21, 2018
Published: October 24, 2018

Abstract

A way is proposed to realize controllable-nuclear fusion by γ-laser or γ-ray and ordinary laser with their certain frequencies and large enough intensities to irradiate a target ball. The function of ordinary laser is to heat the target nuclei and to realize the inertial confinement for the target nuclei. The target nuclei absorbing γ-photons will be in a certain excited state. The scattering cross-sections will be larger and the ignition temperature will be lower to realize fusion of the nuclei in their excited states than those of the nuclei in their ground states. In contrast with the nuclei applied in conventional fusion, e.g., deutons and tritons, according to the way, the nuclei applied to fusion should have the following characters: the nuclei have their excited states, one of the excited states has higher energy and longer lifetime, and the masses of the nuclei are lesser. Thus, the Lawson conditions can more easily be realized so that the controllable nuclear fusion is possibly realized by the way.

Keywords

Controlled Nuclear Fusion, Excited States of a Nucleus, Laser, Interaction of Laser with Matter

1. Introduction

γ-ray has been produced by electron-laser back-scattering. The way to realize γ-laser whose wavelength is continuously adjustable has been presented [1] [2] [3].

To date, controlled nuclear fusion has a important progress [4], but not the ultimate realization. A necessary condition for nuclear fusion is that the Lawson coditions must be satisfied. One of the conditions is that the distance between

two target nuclei must be lesser than the radius of the strong interaction. This means that the nuclear kinetic energy must be large enough to overcome the electrostatic potential barrier between two nuclei. The ignition temperature is not easily achieved by traditional methods.

This paper presents a way to realize nuclear fusion at lower temperature by γ-laser or strong enough γ-ray and ordinary laser to irradiate target atoms. The ignition temperature of nuclear fusion of the excited nuclei is lower, and the scattering cross-section of the excited nuclei is larger. Thus, the Lawson conditions can easily be realized.

The effect of γ-laser or γ-ray is essntially different from the ordinary laser. The energy of a γ-photon can be the same as the difference between these two energy states. Hence a nucleus can transit to its excited state after it absorbs a γ-photon.

In Section 2 the way to realize nuclear fusion by γ-laser is presented; in Section 3, the features of the way are explained; Section 4 is discussion; Section 5 is the conclusion.

2. The Way to Realize Nuclear Fusion by γ-Laser or γ-Ray

1) The Way to Realize Nuclear Fusion by γ-Laser or γ-Ray with Their Large Enough Intensities

Let it have been ready that a target atom ball composed of A and B sorts of atoms, many (such as 36) γ-laser beams or many γ-ray beams with their certain frequency $\omega_{\gamma i}, i = A, B$ and their large enough intensities, and many (such as 192) ordinary laser beams with certain frequencies ω_{oi} and their large enough intensities. The laser beams distribute symmetrically about the target ball and irradiate the target ball. A nucleus absorbing a γ-photon with its energy $E_{\gamma i} = \hbar\omega_{\gamma i}$ will be in its excited state with its energy eigenvalues E_{ei}. Considering the Mossbauer Effect, *i.e.* the recoil effect of the nucleus, we obtain the energy of the photon to be

$$E_{\gamma i} = \left(E_{ei} - E_{gi}\right) + \left(E_{ei} - E_{gi}\right)^2 \Big/ 2m_i c^2,\ E_{ei} \gtrsim T_{eF}, \tag{1}$$

where E_{ei}, E_{gi}, m_i and T_{eF} are the energy of the excited state, the energy of the ground state, the mass of the ith sort of the target nuclei in the static state, and the fusion temperature of the A-nuclei and the B-nuclei in their excited states. In general, the condition $E_{ei} > T_{eF}$ can be satistied. The function of the ordinary laser is to strip the electrons about a nucleus and to realize the inertial confinement for the nuclei in the target ball. In the period of the inertial confinement for the nuclei, γ-laser or γ-ray irradiates the target ball from beginning to end.

It is also possible that the target ball is composed of only the the A sort of atoms. Because of γ-laser or γ-ray irradiation, the target ball becomes a plasma composed of the A-nuclei in their excited states and electrons. When the temperature of the plasma $T_p \lesssim T_{eF}$, incident B-nuclei (e.g. a beam of protons)

with a certain momentum will react with the *A*-nuclei, the fusion of the *A*-nuclei and *B*-nuclei can occur in the plasma.

The reaction of the two nuclei in their excited states has the following features.

The ignition temperature will be lower and the scattering cross-sections will be larger to realize fusion of the nuclei in their excited states.

2) The distance of the nucleons in the outermost shell of a nucleus in its excited state to its nuclear centre is larger than that of the nucleus in its ground state to its nuclear centre

The volume of a nucleus when it is in its excited states is approximately equal to that when it is in its ground state, because a nucleus cannot be compressed. Although the volume of a nucleus is invarient, its shape can change. Because of the stretching action of the nucleus in the outermost shell when a nucleus is in an excited state, a spheric nucleus can become an ellipsoid nucleus when it transits from its ground state to an excited state. In other words, the ratio of the ellisoid long axis to the short axis becomes bigger when the nucleus changes from its ground state to an excited state. Let the long axis and short axis of the ith sort of nuclei in its ground state be r_{gli} and r_{gsi}, the long axis and short axis of the ith sort of nuclei in an excited state be r_{eli} and r_{esi}, respectively, then it is necessary

$$r_{eli} > r_{gli},\ r_{eli}/r_{esi} > r_{gli}/r_{gsi}, \tag{2}$$

Because of (2), there should be

$$l_e > l_g,\ \mu_e > \mu_g, \tag{3}$$

where l_e and μ_e are the orbital angular momenta and the orbital magnetic moments of the nucleus in an excited state, and l_g and μ_g are the orbital angular momenta and the orbital magnetic moments of the nucleus in its ground state.

3) Scattering cross-sections of the strong interaction of the nuclei in their excited states will be larger than that of the nuclei in their ground states

The strong interaction of two nucleons by exchange virtual π-mesons is attractive interaction. Let the strong interaction radius of a nucleon be R_0, then the strong interaction radius of the *A*-nucleus and *B*-nucleus in their excited states is $R_e = R_0 + r_{elA} + r_{elB}$, and the strong interaction radius of the *A* and *B* nuclei in their ground states is $R_g = R_0 + r_{glA} + r_{glB}$. It is necessary that

$$R_e > R_g, \tag{4}$$

because $r_{elA} > r_{glA}$ and $r_{elB} > r_{glB}$.

On the other hand, the surface area of a nucleus in an excited state is bigger than that of the nucleus in its ground state, because their volumes are the same, but $r_{eli} > r_{gli}$. Let σ_g and σ_e are the scattering cross sections of strong interaction of the *A*-nucleus and *B*-nucleus when both are in their ground and when both are their excited states, respectively, then it is necessary

$$\sigma_e > \sigma_g. \tag{5}$$

Increase of scattering cross section is equivalent to increase of the number density n of nuclei.

4) The temperature to realize fusion reaction of the nuclei in their excited states will be lower than that of the nuclei in their ground states

When the distance R_{AB} of the A-nucleus and B-nucleus in their ground states is larger than R_g, *i.e.* $R_{AB} > R_g$, or $R_{AB} > R_e$, the stong interaction between the A-nucleus and B-nucleus may be neglected, When $R_{AB} > R_g$ or $R_{AB} > R_e$, the electromagnetic interaction is dominative. In order to realize the nuclear reaction, $R_{AB} \lesssim R_g$ or $R_{AB} \lesssim R_e$ is necessary. Let Q_A and Q_B are the charges of the A-nucleus and the B-nucleus, respectively, the electromagnetic potential energy between the A-nucleus and the B-nucleus is

$$V_{AB} = Q_A Q_B / R_{AB}. \tag{6}$$

Let E_g be the relative kinetic energy of the A-nucleus and the B-nucleus in their ground states, and E_e be the relative kinetic energy of the A-nucleus and the B-nucleus in their excited states, then only when

$$E_g \gtrsim V_g \equiv Q_A Q_B / R_g, \tag{7}$$

or

$$E_e \gtrsim V_e \equiv Q_A Q_B / R_e, \tag{8}$$

the nuclear reaction of the A-nucleus and B-nucleus can occur. It is obvious that

$$E_g > E_e. \tag{9}$$

In fact, when nuclei are in excited states, the internal energy of the nuclei increase. The internal energy will release out when nuclear reaction occurs. Increase of the internal energy is equivalent to increase of of kinetic energy of the nuclei. Hence the temperature T_e to realize fusion reaction of the nuclei when they are in their excited states will be lower than that when they are in their ground states, *i.e.*

$$T_g > T_e. \tag{10}$$

It is seen from (3), (5) and (10) that the nuclei in an excited state can more easily confined than the nuclei in their ground state. In other words, under the same conditions, the confined time

$$\tau_{ec} > \tau_{gc}.$$

where τ_{ec} and τ_{gc} are the confined times of the nuclei in an excited state and in their ground state, respectively. Consequently,

$$n\tau_e > n\tau_g. \tag{11}$$

Here it is considered that increase of scattering cross section is equivalent to increase of the number density n of nuclei. It is seen that according to the way, the Lawson conditions can easier be realized so that the controlled nuclear fusion can easier be realized.

5) Choice of nuclei applied to fusion and an example

In contrast with the conventional choice of fusion nuclei, it is possible that

deutons and tritons are not optimal nuclei for fusion. It can been seen from above mentioned that the nuclei applied to fusion should have the following characters: the nuclei have their excited states; one of the excited states has higher energy and longer lifetime; and the masses of the nuclei are lesser.

For example, ^{11}B and ^{1}H nuclei may be chosen. The target ball is composed of the $^{11}B_{10}H_{14}$ molecules. Because of irradiation of ordinary laser, the $^{11}B_{10}H_{14}$ molecules is dissociated to plasma composed of ^{11}B's, p's and electrons. It is also possible that the target ball is composed of only the ^{11}B atoms, but proton beams with their large enough momenta impact the target ball. There is the following reaction [5]

$$^{11}\mathrm{B}+\mathrm{p}\to{}^{12}\mathrm{C}^{*}\to{}^{12}\mathrm{C}+\gamma,\ {}^{8}\mathrm{Be}+\alpha+E_{g}',\ 3\alpha+E_{g}. \tag{12}$$

$$^{11}\mathrm{B}+\mathrm{p}\to{}^{11}\mathrm{C}+\mathrm{n},\ {}^{10}\mathrm{B}+\mathrm{d},\ {}^{11}\mathrm{B}+\mathrm{p}, \tag{13}$$

where $^{12}C^{*}$ is an intermediate state or an excited state of ^{12}C, E_{g}' and E_{g} are the energies released in the reaction. Let E_{gp} be the relative kinetic energy of an incident proton and ^{11}B be in its ground state, then when $E_{gp}\lesssim 3\,\mathrm{MeV}$ [5], the reaction

$$^{11}B+\mathrm{p}\to 3\alpha+E_{g},\ E_{g}=8.7\ \mathrm{MeV}, \tag{14}$$

is dominate. There is no neutron to release in the reaction, hence this is a clean fusion-energy sources. But this reaction cross-section is lower and this ignition temperature is higher than those of a deuton and a triton. In order to overcome the two shortcomings, we suggest to irradiate the ^{11}B target nuclei by γ-laser or γ-ray. There is the excited state $^{11}B^{*}$ of ^{11}B whose energy $E_{eB}^{*}=2.124693\,\mathrm{MeV}$ (let the energy of its ground state be zero), lifetime is 3.8 fs, and spin and parity is $(1/2)^{-}$ [5]. The energy of the γ-photon is

$$E_{\gamma}=E_{eB}^{*}+E_{eB}^{*2}\Big/\left(2m_{B}c^{2}\right). \tag{15}$$

E_{eB}^{*} is the transition energy of the ^{11}B nucleus from its ground state with its spin and parity $(3/2)^{-}$ to the excited state $^{11}B^{*}$ when the ^{11}B nucleus is static [5], and m_{B} is the mass of a ^{11}B nucleus. A ^{11}B target nucleus absorbing a γ-photon with its energy E_{γ} will be in its excited state $^{11}B^{*}$ by the interaction of its magnetic dipole $M1$.

$$\gamma+{}^{11}\mathrm{B}\to{}^{11}\mathrm{B}^{*}. \tag{16}$$

To impact a $^{11}B^{*}$ nuclei by such proton with the energy

$$E_{ep}\lesssim\left(3-2.124693\right)\mathrm{MeV}=0.875307\ \mathrm{MeV}, \tag{17}$$

a reactions analogous to (14) will occur, *i.e.*

$$^{11}\mathrm{B}^{*}+\mathrm{p}\to 3\alpha+\tilde{E}. \tag{18}$$

It is seen the ignition temperature will be lower because the relative kinetic energy of a proton and the $^{11}B^{*}$ nucleus reduces from $E_{gp}\sim 3\,\mathrm{MeV}$ to $E_{ep}\sim 0.875307\ \mathrm{MeV}$. Consequently, the fusion temperature will significantly reduce.

The particles in the final states of (18) are the same as those of (14). But The reaction cross-section of $^{11}B^{*}$ + p is larger and this ignition temperature of $^{11}B^{*}$+p is lower than those of ^{11}B+p. When $E_{gp} \lesssim 3\,\text{MeV}$ and ^{11}B in its ground state or when $E_{ep} \lesssim 0.875307\,\text{MeV}$ and ^{11}B in the excited state $^{11}B^{*}$, the probability of the reaction (13) is very small [6]. Especially, there is no neutron to release out in the final states.

It is possible that there are the results analogous to (18) for other nuclei, e.g. $^{11}B^{*}$ + p or $^{9}Be^{*}$ + ^{3}He, here $^{11}B^{**}$ is another excited state of ^{11}B and $^{9}Be^{*}$ is an excited state of ^{9}Be.

Another example is to choose ^{10}B's and neutrons. There are the following reactions

$$^{10}\text{B} + \text{n} \rightarrow {}^{11}\text{B} + E'_{gn}, \tag{19}$$

$$^{10}\text{B}^{*} + \text{n} \rightarrow {}^{11}\text{B} + E'_{en}, \tag{20}$$

It is seen from above described that the reaction (20) is more easilly realized that (19), and the fusion temperature of (20) is significantly smaller than that of (18), because there is no electrostatic potential energy to be overcomed.

3. Discussion

It is possible that the lifetime τ_e of the excited state of target nuclei is shorter than the period τ_{ec} in which the nuclei are confined. For example, the lifetime of the excited state $^{11}B^{*}$ is only 3.8 fs. Thus, it is possible that the nuclei have decayed in the period τ_{ec} so that the nuclei are not in their excited states when two nuclei impact. Thus, it is necessary that γ-laser or γ-ray irradiates the nuclei from beginning to end in the period τ_{ec}. The process in which the nuclei can be in excited states is a dynamic balance process. In order to the $n_e/n_g \gg 1$, the intensity of γ-laser or γ-ray to irradiate the target nuclei should be large enough. It is seen from the process that such excited states which have longer lifetime should be chosen.

The electric field intensity of a laser tail wave. is very strong and variational. When a plasma composed of *A*-nuclei, *B*-nuclei and electrons is confined by a strong magnetic field and is acted by the laser tail wave, the temperature of the plasma will fastly increase. This is because the differences among the mass of a *A*-nucleus, the mass of a *B*-nucleus and the mass of an electron are very large, the differences among the velocities of the *A*-nuclei, the velocities of the *B*-nuclei and the velocities of the electrons and the differences among the accelerations of the *A*-nuclei, the accelerations of the *B*-nuclei and the accelerations of the electrons are all very large so that collision among the *A*-nuclei, the *B*-nuclei and the electrons is very frequent and strong. Consequently, the temperature of the plasma must fastly increase.

4. Conclusion

This paper proposes a way to realize controllable-nuclear fusion by γ-laser or

γ-ray and ordinary laser with their certain frequencies and large enough intensities to irradiate a target ball. The function of ordinary laser is to heat target nuclei and to realize the inertial confinement for the plasma composed of the nuclei and electrons. The target nuclei absorbing γ-photons will be in a certain excited state. The scattering cross-sections will be larger and the ignition temperature will be lower to realize fusion of the nuclei in their excited states than those of the nuclei in their ground states. In contrast with the nuclei applied in conventional fusion, e.g., deutons and tritons, according to the way, the nuclei applied to fusion should have the following characters: the nuclei have their excited states, one of the excited states has higher energy and longer lifetime, and the masses of the nuclei are lesser, for example, ${}^{11}_{5}\mathrm{B}$ and p. On the other hand, it is easier to confine the target nuclei in their excited state because the ignition temperature is lower, and the scattering sections and nuclear magnetic moments are larger. Thus, the Lawson conditions can more easily be realized so that the controllable nuclear fusion is possibly realized by the way.

Acknowledgements

This work is supported by tau-charm physics research KJ (x2-yw-N29) and National Natural Science foundation of China 11075064.

Conflicts of Interest

The authors declare no conflicts of interest regarding the publication of this paper.

References

[1] Chen, S.-H. and Chen, Z.W. (2014) Electron-Photon Backscattering Lasers. *Laser Physics*, **24**, 6.

[2] Chen, S.-H. and Chen, Z.W. (2015) A Discussion on Electron-Photon Backscattering Lasers and the Electron-Photon Backscattering Laser in a Laser Standing Wave cavity. *Laser Physics*, **25**, 5.

[3] Chen, S.-H. and Chen, Z.W. (2016) Coherent Conditions of Electron-Photon Backscattering Light in a Wiggle Magnetic Field. *Laser Physics*, **26**, 5.

[4] Hurricane, O.A., Callahan, D.A., Casey, D.T., *et al.* (2014) Nature, Fuel Gain Exceeding Unity in an Inertially Confined Fusion Implosion. **506**, 343-348.

[5] Firestone, R.B., Shirley, V.S., Frank Chu, S.Y., *et al.* (1996) Table of Isotopes, Eighth Edition, Weily Interscience, Hoboken, 285-313.

[6] Yang, F.J., Wang, Y.S. and Lu, F.Q. (2006) Nuclear Physics. 2nd Edition, Fudan University Press, Shanghai, 295-296. (In Chinese)

Call for Papers

World Journal of Nuclear Science and Technology (WJNST)

ISSN 2161-6795 (Print) ISSN 2161-6809 (Online)
http://www.scirp.org/journal/wjnst

World Journal of Nuclear Science and Technology **(WJNST)** is an international peer-reviewed, open access journal publishing in English original research studies, reviews in all aspects of nuclear science and technology and its applications. Symposia or workshop papers may be published as supplements.

Editor-in-Chief

Prof. Andrzej Grzegorz Chmielewski

Editorial Board

Dr. Abdullah Aydin
Prof. Jiejin Cai
Prof. Ahmet Cengiz
Prof. Abdelmajid Choukri
Prof. Snežana Dragovic
Prof. Hardy Christian Ekberg
Prof. Juan-Luis François
Prof. Shilun Guo
Prof. Shaban Ramadan Mohamed Harb
Prof. Xiaolin Hou
Prof. Ning Liu
Prof. Man Gyun Na
Prof. Dragoslav Nikezic
Dr. Rafael Rodríguez Pérez
Prof. K. Indira Priyadarsini
Prof. Massimo Rogante
Prof. Vitalii D. Rusov
Dr. Chhanda Samanta
Prof. Kune Y. Suh
Prof. Wenxi Tian
Dr. Heiko Timmers
Prof. Marco Túllio Menna Barreto de Vilhena
Dr. Leopoldo A. Pando Zayas

Subject Coverage

This journal invites original research and review papers that address the following issues. Topics of interest include, but are not limited to:

- Fuel Cycle and Isotopes
- Global Nuclear Security Technology
- Nonreactor Nuclear Facilities
- Nuclear and Chemical Waste Management
- Nuclear and Particle Physics
- Nuclear Cardiology
- Nuclear Energy
- Nuclear Engineering and Design
- Nuclear Fusion
- Nuclear Instruments and Methods
- Nuclear Magnetic Resonance Spectroscopy
- Nuclear Materials
- Nuclear Medicine and Biology
- Nuclear Medicine and Molecular Imaging
- Nuclear Physics
- Nuclear Science and Techniques
- Nuclear Structural Engineering
- Nuclear Track Detection
- Nuclear Tracks and Radiation Measurements
- Radiation Applications and Instrumentation
- Radioanalytical and Nuclear Chemistry
- Reactor and Nuclear Systems
- Reactor Science and Technology

We are also interested in short papers (letters) that clearly address a specific problem, and short survey or position papers that sketch the results or problems on a specific topic. Authors of selected short papers would be invited to write a regular paper on the same topic for future issues of the WJNST.

Notes for Intending Authors

Submitted papers should not have been previously published nor be currently under consideration for publication elsewhere. Paper submission will be handled electronically through the website. All papers are refereed through a peer review process. For more details about the submissions, please access the website.

Website and E-mail

http://www.scirp.org/journal/wjnst **E-mail: wjnst@scirp.org**

What is SCIRP?

Scientific Research Publishing (SCIRP) is one of the largest Open Access journal publishers. It is currently publishing more than 200 open access, online, peer-reviewed journals covering a wide range of academic disciplines. SCIRP serves the worldwide academic communities and contributes to the progress and application of science with its publication.

What is Open Access?

All original research papers published by SCIRP are made freely and permanently accessible online immediately upon publication. To be able to provide open access journals, SCIRP defrays operation costs from authors and subscription charges only for its printed version. Open access publishing allows an immediate, worldwide, barrier-free, open access to the full text of research papers, which is in the best interests of the scientific community.

- High visibility for maximum global exposure with open access publishing model
- Rigorous peer review of research papers
- Prompt faster publication with less cost
- Guaranteed targeted, multidisciplinary audience

Scientific Research Publishing

Website: http://www.scirp.org

Subscription: sub@scirp.org

Advertisement: service@scirp.org